

April 2017

Neuromodulation by Mechanical Strain in *C. elegans*

Alexander R. Noonan
Worcester Polytechnic Institute

Benjamin Hatcher Duncan
Worcester Polytechnic Institute

Jacob Roy Maalouf
Worcester Polytechnic Institute

Tristan Oliver Petit
Worcester Polytechnic Institute

Follow this and additional works at: <https://digitalcommons.wpi.edu/mqp-all>

Repository Citation

Noonan, A. R., Duncan, B. H., Maalouf, J. R., & Petit, T. O. (2017). *Neuromodulation by Mechanical Strain in C. elegans*. Retrieved from <https://digitalcommons.wpi.edu/mqp-all/490>

This Unrestricted is brought to you for free and open access by the Major Qualifying Projects at Digital WPI. It has been accepted for inclusion in Major Qualifying Projects (All Years) by an authorized administrator of Digital WPI. For more information, please contact digitalwpi@wpi.edu.

Neuromodulation by Mechanical Strain in *C. elegans*



**A Major Qualifying Project Report Submitted to the Faculty of the
WORCESTER POLYTECHNIC INSTITUTE
In partial fulfillment of the requirements for the Degree of Bachelor of Science**

Benjamin Duncan

Jacob Maalouf

Alexander Noonan

Tristan Petit

Date : April 27, 2017

Approved:

1. *C. elegans*
2. Neural Response
3. Strain

Prof. Dirk Albrecht, Major Advisor

Prof. Songbai Ji, Co-Advisor

This report represents the work of WPI undergraduate students submitted to the faculty as evidence of completion of a degree requirement. WPI routinely publishes these reports on its website without editorial or peer review. For more information about the projects program at WPI, please see <http://www.wpi.edu/academics/ugradstudies/project-learning.html>

Abstract

Current computational models for traumatic brain injury are limited by a lack of understanding of the changes in neuronal function following repeated strain, highlighting the need for large datasets characterizing neuronal response to stretch. To provide a platform capable of gathering these datasets, an apparatus to strain embedded neuronal samples and monitor the subsequent neural response optogenetically was developed. The apparatus enables loading and immobilization of live *Caenorhabditis elegans* specimen, delivers stretch stimulus to the embedded animals, and provides sufficient image resolution to analyze neuronal calcium activity fluorescently both pre- and post-stretch.

Acknowledgements

The team would like to thank Lisa Wall, Elyse Favreau, Kyra Burnett and Laura Aurilio for their help in laboratory and, of course, Professors Dirk Albrecht and Songbai Ji for their advising throughout the project.

Table of Contents

Table of Figures	vi
Table of Tables	vii
Chapter 1: Introduction	1
Chapter 2: Literature Review	6
2.1 Traumatic brain injury (TBI)	6
2.2 TBI Models	8
2.3 <i>C. elegans</i>	10
2.3.1 <i>C. elegans</i> anatomy & nervous system	10
2.4 Imaging	13
2.4.1 Optogenetics	14
2.5 Biomechanics of <i>C. elegans</i>	15
2.5.1 Mechanical properties	15
2.6 Substrates	17
2.6.1 PDMS	17
2.6.2 Hydrogels	18
2.6.3 Polymeric Tubing	20
2.7 Stretching devices	21
Chapter 3: Project Strategy	23
3.1 Initial Client Statement	23
3.2 Design Requirements: Technical	23
3.2.1 Constraints	27
3.2.1.1 Actuating Device	27
3.2.1.2 Substrate	28
3.2.1.3 Monitoring Platform	28
3.2.2 Functions & Specifications	29
3.2.2.1 Functions	29
3.2.2.2 Specifications	30
3.3 Design Requirements: Standards	31
3.4 Revised Client Statement	32
3.5 Management Approach	32

Chapter 4: Design Process	34
4.1 Needs Analysis	34
4.2 Conceptual Design and Feasibility	36
4.2.1 Conceptual Design	36
4.2.2 Feasibility	39
4.2.2.1 Substrate Testing	39
4.2.2.2 Actuation Apparatus Testing	40
4.2.2.3 Initial Feasibility Testing Results	40
4.3 Alternative Designs	41
4.3.1 Alternative Designs for Actuation Device	41
4.3.2 Alternative Substrate Designs	42
4.3.2.1 Silane Glass Cover Slip	42
4.3.2.2 PDMS Slab with Hydration Well	45
4.3.2.3 Tubing with Hydrogel	46
4.3.3 Alternative Designs for Imaging Platform	48
4.4 Final Design Selection	49
4.4.1 Final Design Considerations, Tubing vs. PDMS	49
4.4.2 Final Design Specifications	52
4.4.2.1 Tubing	52
4.4.2.2 Actuator	53
Chapter 5: Design Verification	55
5.1 Tubing Material Selection	55
5.2 Worm Strain	59
5.3 Frame	62
5.4 Neural Response Testing	64
5.4.1 AWA Response Verification	65
5.4.2 AWA Response Experiments	67
Chapter 6: Final Design and Validation	71
6.1 Final Protocol	71
6.2 Design Standards	73
6.3 Economics	73
6.4 Environmental Impact	74
6.5 Societal Influence	75
6.6 Political Ramifications	75

6.7	Ethical Concerns	75
6.8	Health & Safety Issues	76
6.9	Manufacturability	76
6.10	Sustainability	77
Chapter 7: Discussion		78
7.1	Neural Signal Degeneration	78
7.2	Data Limitations	79
7.3	Achievement of Objectives	82
7.3.1	Successful aspects of design	82
7.3.2	Novelty	82
7.3.3	Assumptions	83
7.3.4	Iteration through objectives	83
Chapter 8: Conclusions & Recommendations		84
Appendix A: Neural Response Testing Protocol		89
Appendix B: Arduino Code for Micro Linear Actuator		91
Appendix C: Project Management Plan		93

Table of Figures

FIGURE 1: CALCIUM ACTIVITY MEASUREMENT VIA OPTOGENETICS: (1) CHRIMSON LIGHT OPENS CALCIUM CHANNELS (2) CALCIUM BINDS TO GCAMP (3) GCAMP EMITS GREEN FLUORESCENT LIGHT.....	15
FIGURE 2: CHEMICAL STRUCTURE OF PDMS	17
FIGURE 3: PDMS SLAB [28].....	18
FIGURE 4: PEG MER STRUCTURE	19
FIGURE 5: FEP MER STRUCTURE	20
FIGURE 6: PFA MER STRUCTURE.....	21
FIGURE 7: OBJECTIVE TREE	24
FIGURE 8: SIMPLE SCHEMATIC OF PDMS STRETCHING APPARATUS WITH GLUED HYDROGEL EMBEDDED WITH AN ANIMAL.....	36
FIGURE 9 SCHEMATIC OF UNIAXIAL TENSILE STRESS ON HYDROGEL AND CALCULATION OF APPROXIMATE FORCE REQUIRED TO INDUCE THE REQUIRED STRESS TO APPLY A 30% STRAIN ON A 4000 DA NUMBER AVERAGE MOLECULAR WEIGHT PEGDA HYDROGEL AND THE WORM, ASSUMING UNIFORM BEHAVIOR BETWEEN THE TWO.	37
FIGURE 10: CROSS SECTIONAL AREA CALCULATION FOR TUBING DESIGN (OD = OUTER DIAMETER, ID = INNER DIAMETER)	38
FIGURE 11: IMAGES AND STRAIN RESULTS (PERFORMED IN IMAGEJ®) FOR A STRETCH TRIAL WITH THE SUPERGLUE AND PDMS BASED APPARATUS.....	41
FIGURE 12: SILANE TREATED COVERSIPS AS ANCHOR POINTS WITH A THIRD COVERSIP AS A COVER PREPARED FOR CROSSLINKING.....	43
FIGURE 13: PROOF OF THE STRENGTH OF SILANE TREATED COVERSIP BONDING TO HYDROGEL	44
FIGURE 14: IMAGE OF PDMS SLAB WITH A HYDRATION WELL	44
FIGURE 15: PDMS SLAB WITH GRIPPING BINDER CLIPS TO ATTACH TO LINEAR ACTUATOR	45
FIGURE 16: PDMS WITH HYDROGEL SUCCESSFULLY ATTACHED AND HYDRATION WELL FILLED.....	46
FIGURE 17: WORM IMBEDDED IN 2 MM ID SILICONE TUBING.....	47
FIGURE 18: WORM IMBEDDED IN 2 MM ID SILICONE TUBING SHOWING FLUORESCENCE UNDER NON-IDEAL CONDITIONS.....	47
FIGURE 19: IMMOBILIZED WORM WITHIN A PHOTOCROSSLINKED PEG SEGMENT IN PFA TUBING	56
FIGURE 20: SETUP FOR THE TUBE STRETCH TESTS WITH FIXED END (LEFT) AND STRETCH END (RIGHT).....	57
FIGURE 21: FEP STRETCH RESULTS.....	57
FIGURE 22: PFA STRETCH RESULTS	58
FIGURE 23: FEP AND PDA STRAIN RESPONSE	59
FIGURE 24: TUBE STRETCHING SETUP OVER RHODAMINE FLUORESCENCE	60
FIGURE 25: A SERIES OF WHOLE-BRAIN IMAGING WORMS UNDER RHODAMINE FLUORESCENCE DURING A STRETCH TRIAL IN FEP TUBING.....	61
FIGURE 26: THREE SEPARATE TRIALS OF TUBING STRETCH CORRELATE WITH WORM STRAIN AS MEASURED BY PIXEL COUNT CHANGES IN IMAGEJ®	62
FIGURE 27: INITIAL FRAME PROTOTYPE	63
FIGURE 28: MODIFIED FRAME PROTOTYPE	64
FIGURE 29: FULL SYSTEM ENSEMBLE	65
FIGURE 30: RAW AWA RESPONSE UNDER CHRIMSON STIMULATION. FLUORESCENCE PEAKS AND DESCENTS CORRESPOND WITH EACH RED LIGHT STIMULATION AS INDICATED BY THE RED BARS.....	66
FIGURE 31: AWA RESPONSE UNDER CHRIMSON STIMULATION POST 3.9% STRETCH OF TUBE	67
FIGURE 32: AWA RESPONSE WITH STRETCH. NEURAL ACTIVITY IS MEASURED AS THE CHANGE IN FLUORESCENCE NORMALIZED TO THE INITIAL BASELINE VALUE.....	68
FIGURE 33: AVERAGE PEAK HEIGHT OF AWA NORMALIZED RESPONSE WITH INCREASING TUBE STRAIN	69
FIGURE 34: AVERAGE PEAK HEIGHT OF AWA NORMALIZED RESPONSE WITH INCREASING TUBE STRAIN	70
FIGURE 35: FLUORESCENCE MICROSCOPY OF CHRIMSON-ACTIVATED AWA NEURON (RED BOXES) IN TWO <i>C. ELEGANS</i>	72
FIGURE 36: HYPOTHETICAL NEURAL RESPONSE SCHEMATIC FOR AWA CIRCUIT	79
FIGURE 37: (A) EXAMPLE OF FLUORESCENT IMAGE WITH POOR RESOLUTION AND (B) A POTENTIAL SOLUTION USING A MICROFLUIDIC CHANNEL IN PDMS MASTER IN WHICH TO SEED CROSSLINKED GEL AND ANIMALS.....	80
FIGURE 38: POOR IMAGE RESOLUTION OF THE DVA NEURON	81

Table of Tables

TABLE 1: PAIRWISE COMPARISON CHART FOR “MONITOR RESPONSE” PRIMARY OBJECTIVE	26
TABLE 2: ACTUATING DEVICE CONSTRAINTS.....	27
TABLE 3: SUBSTRATE CONSTRAINTS.....	28
TABLE 4: MONITORING PLATFORM CONSTRAINTS	28
TABLE 5: <i>FUNCTIONS & MEANS ANALYSIS</i>	29
TABLE 6: COMPONENT SPECIFICATIONS	30
TABLE 7: FINAL PROJECT BUDGET.....	33
TABLE 8: CLIENT’S NEED AND WANT CONSIDERATIONS	35
TABLE 9: PDMS VERSUS SILICONE TUBING DESIGN DECISION MATRIX	51
TABLE 10: POLYMERIC TUBING DESIGN SPECIFICATIONS	55
TABLE 11: MAXIMUM STRAIN FOR EACH TRIAL.....	62
TABLE 12: COST ANALYSIS	74

Table of Abbreviations

ASTM	American Society for Testing and Materials International
CFL	confocal
CSK	Cytoskeleton
CTE	Chronic traumatic encephalopathy
DI	Deionized
diSPIM	Dual inverted selective plane illumination microscopy
ECFR	Electronic code of Federal Regulations
EHS	Environmental healthy and safety
FA	Focal adhesion
FEP	Fluoroethylene propylene
FRET	Fluorescence resonance energy transfer
GCaMP	Genetically encoded calcium indicator
ID	Inner diameter
IEEE	Institute of Electrical and Electronics Engineers
IPN	Interpenetrating network
ISO	International Standard Organization
LSFM	Light sheet fluorescence microscopy
NHTSA	National Highway Traffic Safety Administration
NIH	National Institute for Health
NIPAAm	N-isopropyl acrylamide
PDMS	Polydimethylsiloxane
PEG(DA)	Polyethylene glycol (diacrylate)
PFA	Perfluoroalkoxy
TBI	Traumatic brain injury
U.S.	United States
USD	United States dollars
USDOT	United States Department of Transportation
UV	Ultraviolet
ϵ (epsilon)	strain

Authorship

BD = Benjamin Duncan, JM = Jacob Maalouf, AN = Alexander Noonan, TP = Tristan Petit

Chapter 1	BD, JM, AN, TP
Chapter 2	
2.1	BD, TP
2.2	BD, TP
2.3	JM
2.4	AN
2.5	BD
2.6	AN
Chapter 3	
3.1	BD, JM, AN, TP
3.2	BD, JM, AN, TP
3.3	BD, JM, AN, TP
3.4	BD, JM
3.5	BD
Chapter 4	
4.1	AN, TP, JM
4.2	JM, AN, TP
4.3	BD, JM, AN
4.4	TP
Chapter 5	
5.1	BD, JM
5.2	BD
5.3	BD, AN
5.4	BD, TP
Chapter 6	
6.1	TP
6.2	JM, BD
6.3	JM
6.4	AN
6.5	AN
6.6	AN
6.7	JM
6.8	JM
6.9	TP
Chapter 7	
7.1	BD
7.2	AN, JM
7.3	AN, BD, JM, TP
Chapter 8	BD, JM, TP, AN
Appendix	BD, JM, AN, TP

Chapter 1: Introduction

Traumatic brain injury (TBI) is rapidly reaching the forefront of global health concerns. An estimated 1.7 million people in the U.S. sustain a traumatic brain injury every year, with nearly 80% of them requiring an emergency department visit [1]. Annually, there are \$76 billion USD associated with both direct and indirect treatment in the US as estimated by the Center for Disease Control and Prevention [1]. TBI can affect thinking, sensing, language and emotions, but its symptoms are not always apparent nor easy to pinpoint. This is especially true in cases of mild TBI, which accounts for 75% of the total reported injuries, a figure which is likely higher in reality due to probable underreporting in child athlete and military populations [2]. Protective headgear is the standard method of TBI prevention in military and athletic settings. However, the helmets used are designed to prevent skull fracture and commercial products are not validated for preventing damage to soft, sub-cranial brain tissue, which is known to cause long-term neurological impairment [3].

The ability to accurately diagnose, model, and prevent TBI depends on a better understanding of the impact-induced mechanical responses of the brain over a broad range of spatial scales, including the organ, tissue, cellular and subcellular levels. These studies, funded by private institutions and federal grants, are all part of a research market that focuses on improving the health of the nation. These federal grants largely come from sources like the National Institute for Health (NIH), which awarded \$99 million USD towards research in the category of TBI in 2016 [43].

Computational models are increasingly becoming popular in exploring these responses in recent years [2]. However, there are several practical challenges facing current state-of-the-art TBI biomechanical studies. First, there is lack of consensus on the mechanical and material properties of the brain. Different studies have adopted a wide range of material models and property

parameters to characterize brain mechanical behaviors, which makes the accuracy in model-estimated brain responses uncertain. Validation of computational models typically depends on brain-skull relative displacements measured in cadaveric impacts. Data from live human volunteers also exist, but they were acquired from volunteer impacts far below the injurious level. Consequently, even “validated” head models can produce substantially discordant results in brain mechanical responses including strain and strain rate [4].

Another major challenge is the characterization of “injury” itself. A binary definition of injury is typically defined based on strain or strain rate, when their magnitudes are either above or below a predetermined injury threshold. However, there is growing consensus that the brain could experience neurological changes even without a positive diagnosis of injury. This suggests brain functional degradation at lower strain or strain rate levels.

Multiple studies have established biomechanical thresholds for electrophysiological impairment and morphological changes on a tissue-level scale [5], [6], but thresholds for impairment on a single-cell level have yet to be characterized. With this in mind, studying a single neuron’s response to a mechanical stimulus can enhance the general understanding of how TBI-affected neural tissue reacts to different magnitudes and durations of injury. Bar-Kochba et al. recently examined the single-cell effects of applying compressive strains of varying magnitudes and rates to rat neuronal cells in an *in vitro* 3-D model [7], but no studies have examined the effects of tensile strain on single neuronal cells. Neuronal responses to tensile tests are important to analyze since upon impact since neural tissue is known to stretch in tension before undergoing compression against the skull.

The first novelty of our project focuses on building a platform to apply a uniaxial, tensile strain of varying magnitudes and rates to a neural sample. The second is designing a platform that allows for monitoring the subsequent neuronal functional response. The client’s need for this research project is to devise a tool in order to understand the correlation between neuronal

responses and strain. Specifically, this project will seek to analyze single neuronal function throughout strain onset representative of impact as seen in football, boxing, car accidents and other causes of TBI. The current literature pertaining to neuronal trauma has mostly been limited to moderate to severe impacts, opening the door for our research to focus on the effects of milder levels of neuronal strain. In order to replicate these types of impacts, the stress and strain magnitudes must be scaled to represent concussion-inducing forces. This interspecies scaling is especially important when studying a non-mammalian model such as *Caenorhabditis elegans*.

C. elegans is a nematode worm often used as a model organism in neuroscience research for its well-documented nervous system [14]. It is an ideal organism to study because of its resiliency in a variety of cultures and environments. Other characteristics that make this model preferable include: “genetic manipulability, invariant and fully described developmental program, well-characterized genome, short and prolific life cycle, and small body size” [14] [15].

Encapsulating the worm in a hydrogel will allow us to uniaxially strain a target neuron and to measure the strain responses. The benefits of embedding the nematode in a hydrogel is the ease of designing a standardized platform that can be used on all fluorescence imaging platforms. Polyethylene glycol (PEG) based hydrogels have been of particular interest to biomedical engineers within the past decade because of their desirable hydrophilic and biocompatible properties [9] [30]. This project aims to build a working knowledge of mechanical properties pertaining to hydrogels with embedded animals under a variety of applied stresses. The end goal is to create a stretching apparatus that is compatible with a regular light sheet microscope, as well as fluorescence imaging platforms.

The first step of the project strategy is to determine the magnitude and type(s) of mechanical strain to be assessed, such as compressive, tensile, or shear strains and strain rates. Next, an appropriate substrate should be selected that will be compatible with the selected mechanical stimuli and neuronal response imaging, while housing a viable environment for *C.*

elegans. The selected substrate could be based upon naturally occurring biological proteins (collagen), or a synthetic polymer-based hydrogel (i.e. PEG based gels). Then, an apparatus will be designed with the purpose of stimulating the selected hydrogel and *C. elegans* culture with the prescribed mechanical stimulus, while under the observation of a microscope. Finally, one or multiple appropriate methods of monitoring neuronal response will be selected and incorporated. Options for assessing neuronal response include qualitative morphological observations, as well as quantitative data retrieved from either optical readout of intracellular calcium levels, or from electrophysiological monitoring of neuronal graded potentials [10].

It is important to determine criterion for successful achievement of project goals at each stage of the project with quantitative metrics. The first will be to successfully and reliably fabricate the substrate of choice in lab, and be able to successfully maintain viable neuronal culture for at least 24 hours with no mechanical strain applied. Next, the apparatus will have to achieve strains and strain rates representative of various degrees of TBI. Though there is limited data pertaining to tensile strains representative of TBI, researchers have stimulated neurons with a maximum compressive strain for neurons roughly in the range of 0.30, and with compressive strain rates up to 75 s^{-1} [7]. In order to simulate the effects of mild to intermediate TBI, analysis can be conducted at strain rates starting with 1 s^{-1} , 10 s^{-1} , and increasing in increments of 10 up to 80 s^{-1} . Based on a previous study, successful observation of morphological hallmarks after applied strains includes visual presence of neuronal blebbing, contraction, neurite thinning, and eventual cell lysis and death [7]. These preliminary parameters will be used as initial values for design selection, and will be modified as preliminary results dictate. Quantitative optogenetic data should include increases in calcium ion concentration within the cell as a function of cellular damage, though exact thresholds must be established first [10]. Though not a primary objective, a desirable final outcome is that the apparatus as a whole be transferable to different microscope types, such as Dual Inverted Selective Plane Illumination Microscopy (diSPIM) light sheet and confocal light microscopes, and

to different neuronal samples in various types of three dimensional culture. Finally, standards related to working with hydrogels, *C. elegans*, and light-field microscopes from organizations such as IEEE or ASTM must be taken into account throughout the project.

The scope of this project is rooted both in research and design. This project aims to target limitations that are present in current research technology and allow the field of TBI research to advance further. These limitations are mainly present in the type of problems that can be studied in neuronal function. A tool that can study the subtle, intermediate damages to a neuron can give existing computational models a more complete understanding of the physiological and functional impacts incurred by strain. This project's scope is limited to creating this tool and collecting initial data for *C. elegans*, opening the door for more extensive research on potential mammalian models to be done in the future.

Chapter 2: Literature Review

This chapter summarizes relevant background information collected in our research. We focus specifically on traumatic brain injury and its models, *C. elegans*, cell/organism culture substrates for mechanobiological studies, actuating devices, and imaging techniques as they all relate to each other for this project.

2.1 Traumatic brain injury (TBI)

This section explains TBI and its clinical and societal importance with respect to this project.

Traumatic brain injury (TBI) is broadly defined as a type of brain dysfunction as a result of an external mechanical force applied to the head. More specifically, [Medscape.com](https://www.medscape.com) defines TBI as a “non-degenerative, non-congenital insult to the brain from an external mechanical force, possibly leading to permanent or temporary impairment of cognitive, physical, and psychosocial functions, with an associated diminished or altered state of consciousness” [11]. In the United States, an estimated 1.7 million people sustain a TBI annually, while nearly 80% of them require an emergency department visit, and 52,000 incidents end fatally [1]. The leading cause of death in TBI cases is motor vehicle-traffic injury [1], while the vast majority suffers from mild traumatic brain injury, or mTBI.

TBI can complicate the mental functions that affect thinking, sensation, language or emotions. The extent of injury is broadly characterized as “mild” - indicating a brief change in mental status or consciousness, “moderate” - some lesions or abnormalities detected via computed tomography (CT) scans, or “severe” - suggesting an extended period of unconsciousness or amnesia after injury [11]. In civilian populations, mild injury usually comes in the form of a concussion as a result of a head impact in athletics, an automobile accident, or a fall. However,

symptoms of mild injury are not always readily apparent, leading to widespread underreporting especially amongst child and military populations. Individuals who sustain “severe” injury suffer from dramatically debilitated mental function, enter comatose, or die as a result of their injury.

The method of TBI prevention varies among settings, but all current methods function to protect the head from severe impact. Helmets are the most common form of prevention in military and athletic settings, while airbag deployment serves as the primary measure to prevent TBI in the event of automobile accidents. However, neither helmets nor airbags are designed specifically to prevent TBI. The Consumer Product Safety Commission, the national regulatory body for certifying helmets used in sports, validates helmets based only on their ability to prevent skull fracture [12]. The U.S. Department of Transportation (USDOT) requires motor vehicle manufacturers to adhere to Federal Motor Vehicle Safety Standards [50]. The National Highway Traffic Safety Administration (NHTSA) enforces this federal code and approves airbags primarily for their capacity to prevent neck breaks in motor vehicle accidents. Regardless of setting, all current head protection standards fail to protect directly against TBI as their primary function. Protection methods must be improved in the future in order to better prevent TBI which can easily occur without neck or skull fractures.

Given the prevalence and consequences of TBI, it is of great societal importance to determine better preventive and diagnostic tools, as well as treatment methods. This requires more sophisticated understanding of the brain, which is the least understood human organ despite its enormous importance in bodily function.

2.2 TBI Models

This section presents traumatic brain injury models, highlighting what they have accomplished and what can to be done to improve them in the future.

In an attempt to better understand brain injury, scientists have created a wide range of models to simulate and monitor the effects of TBI on brain tissue. They can be divided into two camps - physical models and computational models. Physical models include cadavers, dummies human volunteers, and animal models with which experimenters attempt to replicate the mechanical environment of traumatic injury on their subjects. Cadaver models have the advantage of being able to undergo accurate injury simulation, especially with respect to impact magnitude and direction. However, the results of these impacts only indicate results relating to mechanical deformation of brain tissue. Moreover, only high-end severe injury situations have been examined to date, failing to give any insight into the mechanical outcomes of milder injury.

Experiments on human volunteers are the most realistic TBI model, but are greatly limited by a lack of necessary imaging and sensing capabilities and confinement to the low end of the injury spectrum for ethical reasons. There are limited research projects and published literature on this type of TBI model. Currently there is no method to induce TBI on a human without actually inducing injury. If human models could induce TBI without injuring the affected people, they would be considered the new state of the art in this field.

Meaney et al. (2003) studied several civilian and military cases of TBI by characterizing the severity, the type (blast-related or not) and the cause (motor vehicle accident, fall, etc.). Defining the scope of a TBI is an important step in diagnosis and treatment because the severity, type, and cause all play a large role in the mechanical response in the brain. This study examined the effect of human connectome i.e. measuring the directional changes of white matter tracts in the

brain changing with blood flow. Since the brain has such a complex geometry, the main method of studying these types of injuries began with experimental models of either a physical surrogate, human, or animate. Once enough information from these models was collected, researchers began developing computational models that took into account complex conditions that the physical models could not e.g. soft brain material properties, structure, etc. One key problem that arises in computational models is the soft material properties coupled with the incompressible dilatational nature of the brain.

The greatest insights into the effects on neural tissues has come from the result of animal models. Bain et al. (2001) studied the morphological and electrophysiological effects of stretching the optic nerve in a guinea pig [6]. Functional impairment of the nerve due to mechanical stimulation was characterized by electrical potentials from the optic nerve to the brain. Morphological effects were characterized after death and recovery of all optic nerves via a binary system. A score of 0 or 1 was assigned to each nerve based on absence or presence (respectively) of axonal swellings or retraction bulbs in any part of the nerve.

Dummies represent the gold standard for determining the physical parameters (force and acceleration) required to induce severe injury in physical models. Additionally, other physical models such as cadavers from dead animals can help researchers determine the material properties of mammalian brains. However, the main limitation of defining tissue level parameters of lifeless physical models is that the required amount of strain and strain rate to produce injury is not available. Computational models allow researchers to input mechanical properties from physical models, and use finite element analysis to obtain the strain and strain rates produced from a simulated traumatic impact. Current computational models lack the predictive power to determine the biologic effects of moderate trauma, which can be indicative of chronic, long term conditions such as Chronic Traumatic Encephalopathy (CTE). A method to produce datasets characterizing single cellular effects would fill the informational gap in current computational models. This

would allow them to not only predict what forces are required to produce a severe hemorrhage and extensive tissue death, but moderate chronic effects as well. An appropriate system must be used in order to derive relevant data. Brain slices would provide a suitable neuronal culture, which can be embedded for compressive and tensile tests. However, maintaining a culture of brain slices while simultaneously performing mechanical tests confounds experimental difficulty as well as complicating variables to data collection. Additionally, the use of neuronal cultures involves a singular culture of one cell type - not a realistic representation of the other cell types which could influence stretch response. A heterogeneous medium of neuronal cell types more representative of mammalian brain composition can be found in a self-contained model organism, as opposed to neuronal cultures. An ideal system, therefore, would involve experiments on whole organisms rather than cell cultures. The model organism we have selected for experimentation is *C. elegans*.

2.3 *C. elegans*

This section introduces Caenorhabditis elegans, a nematode whose nervous system has been extensively studied for several decades. Emphasis is put on what makes it a good model organism for this project's goal and how it has already been used in TBI research.

2.3.1 *C. elegans* anatomy & nervous system

C. elegans nematodes are transparent worms that live on a diet of *E. coli*. They reproduce both sexually and asexually, with their young maturing in three days and living for up to two to three weeks. Adults are roughly one millimeter in length [14] [15]. For all of these characteristics, they are easy to maintain in a laboratory setting.

C. elegans is most famous for the role it has played as a model organism in neuroscience research, being the first multicellular organism with a completely sequenced genome. Through decades of research, scientists have compiled data on the males' 385 and the hermaphrodite's 302 neurons on websites such as wormatlas.org and wormbase.org. Other databases collect and make available genetic information, protein expression data, open reading frames (ORFs) and behavioral

data [14]. These collaborative and public databases serve as excellent tools for understanding *C. elegans* and identifying candidate neurons to study in experiments such as ours. *C. elegans* is the only organism with a fully mapped connectome, making it highly desirable for monitoring the interactions between different neurons and neural communication circuits [15]. Since it is well studied within the scientific community, many lines expressing a variety of different neuronal imaging targets are readily available. This is critical to the development of this project, since the responses to a variety of different neuron types and anatomical orientation can be tested for injury response. *C. elegans* is also unique in that, from one animal to the next, neuronal anatomical location, function, and response can be expected to be consistent [15]. The level of consistency that can be achieved with *C. elegans* data is therefore unparalleled. The variety of testing which can be conducted adds another facet of desirability compared to testing brain slice cultures, in addition to ease of culture.

Like its mammalian neurochemical homologues, *C. elegans* has a variety of neuron types which differ in functional capacity. The three neuron types are sensory neurons, motor neurons, and interneurons [16]. Analyzing the functional response in each type can provide a different dimension to understand the mechanisms of neuronal injury and for setting up appropriate controls. Neurochemical signals can travel through three different types of synapses: chemical synapses, gap junctions, and neuromuscular junctions. *C. elegans* has 6400 chemical synapses, 900 gap junctions, and 1500 neuromuscular junctions [17]. Additionally, 75% of the chemical synapses in hermaphrodites are reproducible from animal to animal, highlighting *C. elegans*'s unique homology and consistency which is ideal for experimentation [15]. Chemical neurotransmitters are important to consider as a mode of interneuronal communication, given that neurotransmission could be compromised by strain applied to the animal and that chemical synapses comprise the majority of neuronal communication mechanisms. When a nerve is stimulated, voltage gated calcium channels in the nerve terminal are activated, causing a massive influx of Ca^{2+} ions. The

high concentration of Ca^{2+} within the cell triggers the formation of synaptic vesicles, which fuse with the next presynaptic membrane - activating the next nerve cell [18]. Damage inducing strain to neurons could be expected to alter activity in the presynaptic neuron, as well as affecting the activity of other neurons within that circuit. Therefore, not only can changes in response within the same neuron be measured, but analysis of downstream changes can add to a comprehensive understanding of the total effects due to strain.

For the purposes of analyzing a single neuron for initial tests, specific neurons can be selected based on their anatomical location and function. The DVA neuron is a stretch-sensitive sensory neuron that runs along the length of the worm and is known to have stretch sensitivity that provides input to both anterior and posterior touch circuits [16]. Due to its properties as a stretch receptor, DVA would serve as a positive control for response to uniaxial strain on a developed experimental setup. Needless to say, however, that its response would not be applicable to a human TBI simulation since there are no stretch receptors in the human brain. Therefore, an ideal neuron to isolate for the purpose of TBI studies would run along the ventral cord of the worm like the DVA proprioceptor. Another neuron which could be tested is AWA, an olfactory (odor sensitive) neuron which is sensitive to volatile odors such as diacetyl. When AWA detects an odor, calcium levels increase to an easily detectable level within the cell, suggesting a depolarization due to voltage gated calcium channel activity [20]. Because AWA is olfactory and would not be expected to respond to proprioceptive triggering forces, it can serve as an experimental neuron; a change in its response could therefore be due to damage, not a normal stretch response. It also fits the criterion of running longitudinally relative to the orientation of the worm, allowing a uniaxial strain to be translated accordingly.

2.4 Imaging

This section describes the principles of imaging techniques that are considered for use in this project, with a focus on neural imaging and monitoring methods.

The monitoring of neural activity in live time has long been a challenge in research. Since the conduction of nerves is electrical in nature, it is possible to observe the charge difference with electrodes. The advantage is that the signal can be detected at a distance from the source resulting in a minimally invasive method that can be used for applications such as measuring brain activity. The major drawbacks are that invasive procedures are needed for implementation and it can be prone to signal noise if movement and electromagnetic interferences from motors are introduced [18]. Another method of capturing neuronal activity is to monitor calcium ion levels across neuronal cell membranes. Essentially, this is accomplished through monitoring of free calcium levels on the inside of the membrane. Calcium imaging has been progressing with the limiting factors being the calcium sensor technology and the instrumentation available. The first calcium indicators used were bioluminescent calcium-binding photoproteins such as aequorin that were used to monitor the dynamics of cellular calcium signaling. The implementation of these techniques was often tedious because of the dye delivery [18]. Utilizing the advantages of genetic engineering in simple organisms it is possible to encode fluorescent calcium reporters in the neurons of interest, which are easily detectable with wide field fluorescence microscopy techniques in live time. One common technique of fluorescence-based optogenetic monitoring involves fluorescence resonance energy transfer (FRET), in which a donor fluorophore excites an acceptor leaving the donor at a ground state. FRET has been used *in vitro* for studying neuronal calcium activity [21], [22], as well as for *in vivo* imaging of *C. elegans* mechanosensory neurons [24]. Alternatively, GCaMP proteins are non-FRET and rely only on conformational changes to

fluoresce [49]. It is possible to express GCaMP in different neurons such that behavioral changes can be correlated with neuronal activity [20] [48] [49].

2.4.1 Optogenetics

Optogenetics is the practice of genetically engineering cells or organisms to express photochromic molecules in target proteins. These photochromic molecules are light sensitive and can be activated or silenced with light. Photochromic molecules can be ion channels in which light exposure causes the opening of those channels, such as the blue-light sensitive channelrhodopsin cation channel [47]. Photochromic molecules can also be tailored to express sensitivity to specific wavelengths of light such as Chrimson, a red-light sensitive variant of channelrhodopsin [21]. Through the use of optogenetics, the function of a neuron can be quantifiably observed. This can be accomplished using fluorescent GCaMP proteins that change their conformation when calcium binds to them. This conformational change causes the molecule to fluoresce. The fluorescence from the activated GCaMP can then be quantified through the use of imaging software [25]. Change in fluorescence can then be correlated to the change in function of a neuron in relation to the experimental conditions.

In our experiment we make use of a genetically engineered line of *C. elegans* that includes a coexpression of the red-shifted Chrimson cation channel with GCaMP2.2b in AWA. Red light excites Chrimson to depolarize AWA and blue light excites GCaMP2.2b in AWA [21]. The following numbers correspond to the diagram below. 1: The Chrimson ion channel is red-light sensitive meaning that exposure to red light will cause it to open and conduct cations. 2: The open channels cause a flux of cations such as H⁺, Na⁺, K⁺, and Ca⁺⁺, locally depolarizing the neuron. Other voltage-gated channels may open, depolarizing other regions of the neuron. 3. Intracellular calcium, from internal and external sources, interacts with the GCaMP expressed within the cell. The GCaMP protein changes conformation and when excited by blue light, emits green

fluorescence with an intensity that correlates with calcium concentration, and generally with neural activation.

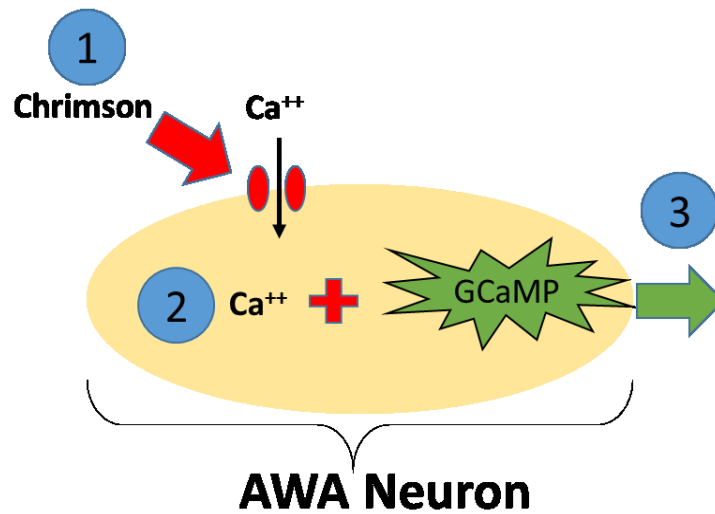


Figure 1: Calcium activity measurement via optogenetics: (1) Chrimson light opens calcium channels (2) Calcium binds to GCaMP (3) GCaMP emits green fluorescent light

2.5 Biomechanics of *C. elegans*

Due to the aforementioned advantages of studying *C. elegans* as well as the mechano-transductive analogues that have been discovered between it and the human nervous system [26], scientists have at many times used these worms as biomechanical models. Furthermore, the family of animal models investigated in TBI research happens to include *C. elegans*. First, we will summarize studies pertaining to *C. elegans* neural circuits. We will then summarize the findings of biomechanical studies of *C. elegans*, including those used as a TBI model.

2.5.1 Mechanical properties

Research in the area of the overall mechanical properties of *C. elegans* has been generally limited. Gilpin et al determined the bulk mechanical properties of worms using an apparatus designed to apply hydrostatic compressive and tensile forces [27]. They determined the average bulk modulus to be $\kappa = 140 \pm 20$ kPa (N=22). Additionally, they found that enzymatic treatment of

worms to degrade cuticle proteins did not result in a statistically different modulus ($\kappa = 130 \pm 50$ kPa). The negligible influence on modulus suggests that the cuticle does not insignificantly contribute to the bulk mechanical properties of *C. elegans*. Instead, internal structures would seem to be the determining factor of worm modulus. Therefore, stretching of the worm would likely to translate directly into stretching of the internal structures.

Another method used in *C. elegans* body mechanics research is the use of a piezoresistive cantilever to directly stretch a worm placed on a glass slide [8]. The benefits of this system include the ability to apply a large range of different forces, and the ability to measure these microscale forces without optical methods, but rather through an integrated readout. The group found that *C. elegans* demonstrated linear elastic force-displacement behavior. They found that internal hydrostatic pressure contributes minimally to mechanical properties, while the cuticle contributes significantly. The stiffness determined was on the order of 0.801 N/m. They modeled the worms as a long cylinder in order to produce theoretical values for stiffness and modulus, and estimate the theoretical contributions that hydrostatic pressure and the cuticle contribute to the overall stiffness.

Angstman et al. acknowledged the gap in mild blast related TBI (br-mTBI) research by demonstrating the effects of shock wave exposure on *C. elegans* locomotion [27]. Though the effects of secondary and tertiary blast waves are easily studied, the effects of primary blast waves are difficult to characterize. This research group focused on developing a high throughput method for studying solely the effects of primary blast waves and cavitation. Their study is of particular interest due to the bridging of *C. elegans* experiments to human mild TBI models, and their use of locomotion to determine injured neuronal functionality.

2.6 Substrates

This section describes the various polymeric solids, referred to as “substrates” throughout this report, that are used to house *C. elegans* in research.

2.6.1 PDMS

Poly(dimethylsiloxane) (PDMS), an organic siloxane elastomer, is considered the substrate material of choice for most microfluidic experiments involving *C. elegans* for its wide range in material properties and low cost. Its siloxane bonds enable a high degree of chain flexibility and viscoelasticity, also making it suitable for mechanobiological studies [28].

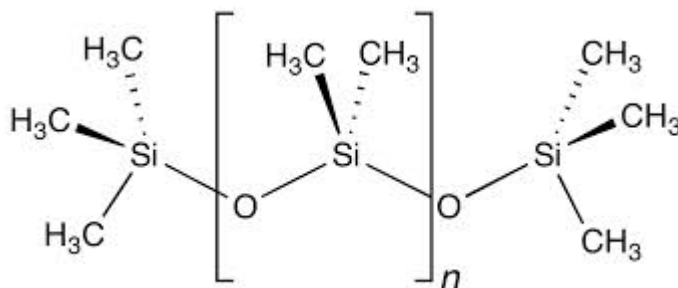


Figure 2: Chemical Structure of PDMS

PDMS is transparent at optical frequencies between 240 nm and 1100 nm and has low autofluorescence, facilitating its use when imaging biological samples [29]. PDMS is considered biocompatible due to its low toxicity, but hydrophobicity on its surface permits adsorption of negatively charged proteins that can mediate negative biological reactions. However, silanol terminations can make the PDMS surface hydrophilic for up to around 30 minutes, allowing resistance to negatively charged particles [29].

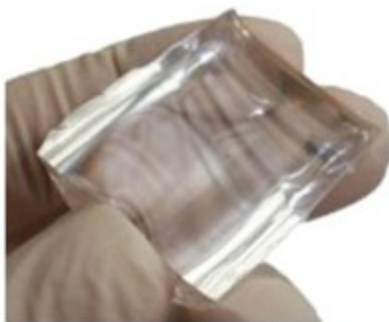


Figure 3: PDMS slab [28]

PDMS' high degree of permeability to atmospheric oxygen (O_2), carbon dioxide (CO_2) and water vapor make it useful in cell culture applications, but can negatively affect the control of chemical gradients and volumes. Markov found that surface gas permeability can be varied through surface plasma treatment (parylene and paraffin wax coatings) and controlling storage conditions [29].

2.6.2 Hydrogels

Hydrogels are polymeric materials capable of swelling with water and maintaining a distinct three-dimensional shape. Due to their fluid retention and ability to interact biologically [30] they are often employed as cell culture substrates. Despite this, current hydrogels lack the mechanical properties needed to sustain the strains used in mechanobiological studies of embedded cells and organisms.

Researchers have explored a variety of approaches in improving the mechanical properties of hydrogels. Okumura and Ito (2001) [31] achieved a high stretching ratio and high degree of swelling in water through the use of sliding crosslinking agents, which involves the chemical crosslinking of two cyclodextrin molecules, each threaded on a different polyethylene glycol (PEG) chain and end-capped with a bulky chain group such as adamantane. Alternatively, Haraguchi [32] radically polymerized a clay-filled hydrogel nanocomposite of NIPAAm and

hectorite that was able to elongate up to 1500%. Furthermore, hydrogels' molecular architectures have been varied, such as the double interpenetrating networks (IPNs) formed by Gong [33] to create a highly tough and hard gel. Superporous hybrid (SPH) gels have also been reported as very tough when stretched [34], but high porosity may not be suitable in cases where an embedded organism needs to be immobilized within a crosslinked gel. Yun Sun et al [35] produced highly tough and stretchable alginate and polyacrylamide-based hydrogels.

Polyethylene glycol (PEG) is a hydrogel material often used for *C. elegans* research due to its hydrophilicity, biocompatibility and resistance to protein adsorption [37].



Figure 4: PEG mer structure

PEG hydrogels can be fabricated via bulk polymerization using an ultraviolet (UV) radiation source and crosslinking agent. Although this method of photopolymerization can theoretically produce relatively pure and initiator-free hydrogels [36], the issue of oxygen inhibition can compromise gel properties and performance. Molecular oxygen inhibits photopolymerization by reacting with initiator, primary and polymer radicals to form peroxy radicals which do not reinitiate polymerization, thus reducing reaction efficiency. This likely occurs on substrate surfaces, forming an unpolymerized, tacky top layer with reduced surface and optical properties [37].

Torgensen et al. recently used a two-photon (2PP) 3D laser fabrication to manufacture a photo-sensitive PEG diacrylate (PEGDA) gel. Their 200 x 200 x 35 μm scaffold can hold up to 80% water content and is capable of embedding *C. elegans* worms. A correlation was established between increased water content and worm survival rate [51]. Interestingly, Zheng [38] devised a

PEG gel that polymerizes during strain onset, known as a strain-promoted crosslinking wherein the hydrogel network forms via copper-free cycloaddition according to the rate and amplitude of an applied strain.

2.6.3 Polymeric Tubing

Polymer-based tubing can have a wide variety of compositions and applications, depending on their properties. For the purposes of this project, they could serve as a housing for a crosslinked gel to be stretched. Though silicone tubing could be useful, polymeric tubing has more tunable properties which could be of importance to this project [45].

Two teflon derived copolymers were examined for their applicability to favorable crosslinking conditions, optical properties, and ability to stretch. Fluorine ethylene propylene (FEP) is one such copolymer (Figure 4).

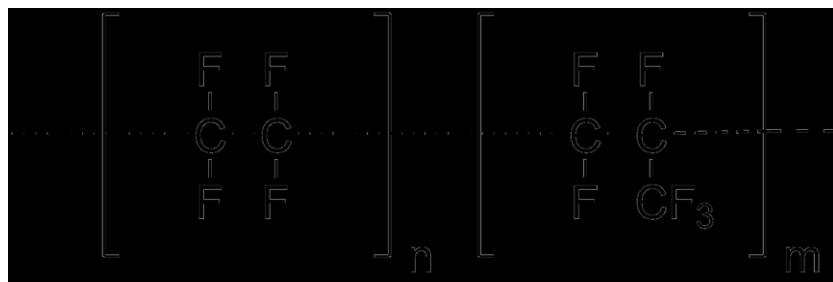


Figure 5: FEP mer structure

FEP is chemically inert, making it ideal for situations where the solvent within the tube must not react, and where gas permeability to the outside must be little to non-existent. Another key benefit of the material is it has the closest refractive index to water of all thermoplastics, making it ideal for imaging purposes [45].

PerFluoroAlkoxy (PFA) is another fluoropolymer related to FEP, with the addition of an alkoxy group (Figure 5). It is generally used for many of the same applications as FEP, but is generally more adaptable to hostile chemical and physical environments including mechanical

stress, high heat, and harsh chemicals. Though this could result in low stretching ability, the material could also be less permeable to outside gasses, including oxygen [45]. The feasibility of crosslinking within both materials would have to be compared in order to evaluate oxygen permeability in material selection.

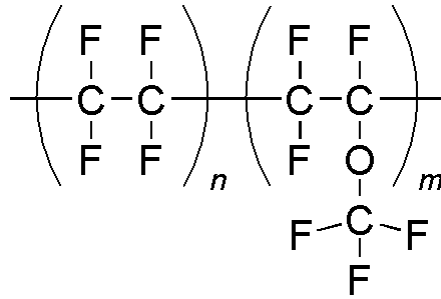


Figure 6: PFA mer structure

2.7 Stretching devices

This section details the methods of actuation and the techniques that have been used to stretch cell and organism cultures.

There are many ways of creating linear actuation. The commercially available options include three main deviations; pneumatic, hydraulic, and electric types of linear actuation. In the case of pneumatic actuation, air is used to drive a piston. Hydraulic actuation uses an incompressible fluid such as water. In the case of the electrical actuation, electrical energy is converted into torque that is transferred to a screw. The advantages of pneumatic actuation are that they can generate precise linear motion that is within 0.1 inches and repeatability within 0.001 inches. Pneumatic actuators have seen advances in miniaturization in recent years and have the advantage of being lightweight and relatively low maintenance. The disadvantage of pneumatic actuation is that pressure losses in the lines can lead to unexpected low forces. Another disadvantage is that the compressor must be constantly running even if the actuator is not in motion. The advantages of a hydraulic system are that the compressors do not always need to run due to the incompressibility of the fluids. Also the forces generated are larger. The advantages also

include the fact that the pumps or motors can be located further from the actuator with minimal loss of power. Like a pneumatic actuator the disadvantage can be that a loss of fluid will lead to a loss of efficiency, but the fluid leaked can cause damage to surrounding components. Another disadvantage to hydraulic actuators are their unwieldy sizes due to their many companion components that include fluid reservoir, motors, pumps, release valves, and heat exchangers, along with noise-reduction equipment. Electrical actuators offer the highest precision-control positioning. These actuators can have an accuracy of ± 0.000315 in. with a repeatability of less than 0.0000394 in. Their setups are scalable for any purpose or force requirement, and are quiet, smooth, and repeatable. Electrical actuators are easily programmable and provide instant feedback and maintenance information. Because of the lack of fluid, the hazards to other components of the system are minimized. The disadvantages to an electrical actuator are that the initial cost may be higher than a pneumatic or hydraulic system. Also, the motor cannot run continually since it can overheat. The electrical actuator's parameters are also limited to the fixed settings chosen at the time of purchase [41].

Cell stretchers are devices that make use of linear actuators to stretch a microenvironment for a variety of purposes. The environment that a cell is being cultured in can determine its function and form. To accurately mimic an *in vivo* environment *in vitro* allows for a more controlled culture of cells while maintaining the cell's native environment (*Strex*). The reason this is true is because intracellular behaviors can be driven by extracellular stimulation. Mechanosensation and mechanotransduction pathways such as F - actin cytoskeleton (CSK) structures and focal adhesions (FAs) anchoring F - actin CSK to the extracellular environment are two main mechanoresponsive structures created by cells. Understanding the behavior in response to cell stretching of these structures is of great importance in furthering the understanding of mechanobiology and mechanotransduction.

Chapter 3: Project Strategy

The following chapter outlines the strategy of this project including project objectives, constraints, functions, specifications, and standards that will be taken into account.

3.1 *Initial Client Statement*

The client statement expresses the needs that the client expects this project to address.

The client provided the following statement at the project debut:

“Devise a system to measure changes to neural response with strain.”

3.2 *Design Requirements: Technical*

The initial client statement can be broken down into two ranked primary objectives:

1. *Build and implement an apparatus to induce mechanical trauma in C. elegans neurons*
2. *Monitor neural response on a single-cell basis*

First and foremost, the devised system must simulate a mechanical environment characteristic of traumatic brain injury. Next, the neural response must be monitored both qualitatively and quantitatively in order to produce the desired data correlating neuronal function and strain. The following objective tree presents these two primary objectives as well as their sub-objectives (Figure 5).

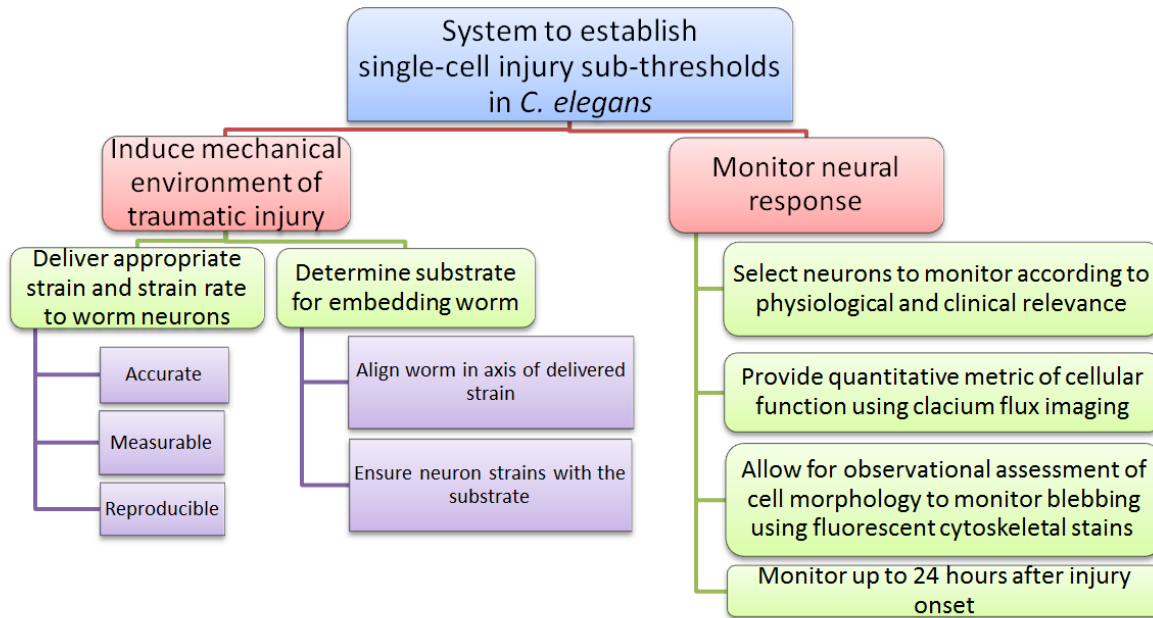


Figure 7: Objective tree

Given the constraint of the microscale size of the worm, the client recommended the use of a substrate in which to embed the worm, which will serve as a stretchable platform to make it more practical to induce mechanical strain. The selection and characterization of this substrate, along with the effective delivery of appropriate strains and strain rates to the neuron, serve as the sub-objectives of the first primary objective to simulate the mechanical environment of traumatic injury.

Specifically, the delivered mechanical strain must be accurate, measurable and reproducible. The measurability of these values is determined by features of the mechanism providing the actuation. For example, strain can be estimated as the displacement measured by a linear displacement transducer attached to an actuating device. Likewise, it can be calculated from real-time data provided by a force transducer in a similar device. Regardless of the means of actuation, the actuating device must provide either a direct measure of strain or a related metric (e.g. force, stress, displacement) that can be used to approximate strain and strain rate. These measurements must be accurate, so that the actuation device can deliver the desired strain and

strain rate values. Lastly, the mechanism that actuates the substrate and worm compound must be able to repeatedly achieve this with a degree of accuracy.

The selected substrate must match the demands in mechanical properties while satisfying the demands of the worm. The substrate will need to strain at the established magnitudes and rates without failure. Furthermore, it must be compatible with *C. elegans* and allow for the worm to be embedded such that it can align along the strain axis. Lastly, it must have a certain degree of adherence to the worm to ensure that the worms' neurons strain with it during actuation, and if not, establish a baseline set of correlation values between gel and worm stretch to create a correlation curve between the amount of stress the actuator applies, and the strain that will be applied to the worm.

With regards to the second primary objective, there are several sub-objectives in monitoring the neural response of the worm. These include selecting a neuron to monitor within the *C. elegans* based on physiological and clinical needs, providing a quantitative metric for the function of the neuron, allowing for qualitative assessment of morphology and behavior, and monitor up to 24 hours after injury onset.

These sub-objectives can be ranked with the aid of visual tools like Pairwise Comparison Charts (PCCs). PCCs rank objectives by assigning values to the objectives against each other: 1 if more important, 0.5 if equally important, and 0 if less important. Then, totals are calculated horizontally to provide a final score for each objective. Table 2 provides a pairwise assessment of the sub-objectives of monitoring the neural response.

Table 1: Pairwise Comparison Chart for “Monitor Response” Primary Objective

OBJECTIVE	Select neuron	Quantitative metric of cellular function	Qualitative assessment “ “	Monitor up to 24 hours	TOTAL
Select neuron		0	1	1	2
Quantitative metric of cellular function	1		1	1	3
Qualitative assessment “ “	0	0		1	1
Monitor up to 24 hours	0	0	0		0

The most important factor in deciding which neuron to monitor is the anatomical position. It is best to focus on a neuron that runs from the head to the tail of the worm while inducing tensile strain. Clinically, it is also important to choose a neuron type that can be representative of both a proprioceptive control, as well as an interneuron, since the human brain does not contain proprioceptive neurons. It is important to quantitatively monitor the mechanical response to the chosen neuron of *C. elegans* to obtain datasets for tensile stresses. New datasets would enhance computational models by adding tangible data to the programs that allow researchers to produce models of TBI. The qualitative aspect of the data is important to compare with existing literature to categorize subthreshold (mild) injuries versus post cell lysis (severe) injuries. The neuronal response to repetitive subthreshold injuries for extended periods has not been observed before. Monitoring these responses for up to 24 hours, to observe for late stage effects, is crucial to enhancing understanding of neuronal response to repeated strains.

In summary, the primary objectives and sub-objectives, ordered by decreasing levels of importance, are:

- ❑ ***Build and implement an apparatus to induce mechanical trauma in C. elegans neurons***
 1. *Deliver 10% strain to worm neurons*
 2. *Determine substrate and workflow for embedding worm*
- ❑ ***Monitor neural response on a single-cell basis***
 1. *Provide quantitative metric of cellular function using calcium ion flux imaging*
 2. *Select neurons to monitor according to physiological relevance*
 3. *Allow for observational assessment of cell morphology to monitor blebbing*
 4. *Monitor up to 24 hours after injury onset*

3.2.1 Constraints

Since the system to be designed consists of three major components (the actuating device, substrate, monitoring platform), the project's constraints pertaining to each component are presented in the following subsections.

3.2.1.1 Actuating Device

The constraints of the actuating device are:

Table 2: Actuating Device constraints

<u>Constraint</u>	<u>Rationale</u>
<i>Grip to substrate ends</i>	PDMS slab design will have cross sectional dimensions of 17.0 x 1.4 mm, and polymeric tubing an inner diameter of 0.5 mm
<i>Deliver 4.4 - 7.3 N (minimum lower bound for PDMS and polymeric tubing, respectively) (see Figure 5 in Chapter 4.2)</i>	Estimated value of force needed to strain a PDMS slab (based on stress-strain curves for Sylgard 184) or for PFA tubing (based on Young's modulus and cross-sectional area). .
<i>Actuate up to 4.4 mm (minimum lower bound) in displacement</i>	An actuation of 4.4 mm in displacement correlates to the prescribed maximum strain of 10% and the 44 mm length of the PDMS slab substrate.

3.2.1.2 Substrate

The constraints of the substrate are given in the following table:

Table 3: Substrate constraints

<u>Constraint</u>	<u>Rationale</u>
<i>Strain up to 10% without failure</i>	The hydrogel must reach this strain without failing in order to ensure results of the experiment can be collected from the worm that is housed within and being strained equally
<i>Maintain <i>C. elegans</i> viability for a minimum of 24 hours</i>	This ensures that both that worms remain observable on the 2-3 hour post-injury time scale demanded by the client, and that worm death occurs more likely as a result of injury than an age-related cause
<i>Simple workflow for mounting worms</i>	Allows for reproducible data collection in an efficient process

3.2.1.3 Monitoring Platform

The constraints of the monitoring platform are:

Table 4: Monitoring platform constraints

<u>Constraint</u>	<u>Rationale</u>
<i>Minimum field of view 3 mm x 3 mm</i>	The 1 mm length of the animal must be fully visible at 10x magnification in order to allow for quantifiable and clear neuronal imaging.

3.2.2 Functions & Specifications

3.2.2.1 Functions

The table below details the functions of the designed system with possible means for accomplishing each function.

Table 5: Functions & Means Analysis

<u>Function</u>	<u>Means</u>
Induce tensile strain on worm	<ul style="list-style-type: none"> <input type="checkbox"/> Electrically powered actuator <input type="checkbox"/> Piezoelectric stimulation of substrate <input type="checkbox"/> Negative hydrostatic pressure in microfluidic channel
Quantify induced strain	<ul style="list-style-type: none"> <input type="checkbox"/> Readout from actuating device (e.g. force sensor, linear displacement transducer) <input type="checkbox"/> Estimate displacement of marker embedded in substrate under microscope (e.g. microbeads)
Quantify neural response	<ul style="list-style-type: none"> <input type="checkbox"/> Optogenetic marking of Ca channel activity <input type="checkbox"/> Action potential measurement by electrodes attached to worm <input type="checkbox"/> Behavioral response metric (e.g. locomotion, head swings)

3.2.2.2 Specifications

The various components of the project must meet certain specifications, detailed below, with respect to the constraints and needs established above.

Table 6: Component Specifications

Component	Specification
<i>Actuating device</i>	<input type="checkbox"/> Induce up to 10% strain in substrate <input type="checkbox"/> Apply adjustable strain rates
<i>Substrate</i>	<input type="checkbox"/> Ability to strain up to 10% and at maximum rate of 10 s ⁻¹ without plastic deformation <input type="checkbox"/> Biocompatible with <i>C. elegans</i> <input type="checkbox"/> Manufacturable to 4.4 mm * 1.7 mm * 0.14 mm size <input type="checkbox"/> Preserve worm viability for at least 24 hours <input type="checkbox"/> Immobilize worm along strain axis <input type="checkbox"/> Transparent for imaging
<i>Monitoring platform</i>	<input type="checkbox"/> Minimum field of view 3 mm x 3 mm <input type="checkbox"/> Able to quantify change in fluorescence ($\Delta f/f_0$)
<i>Tubing</i>	<input type="checkbox"/> Small inner diameter (~0.02 in) <input type="checkbox"/> Optically transparent <input type="checkbox"/> UV transparent <input type="checkbox"/> Stretchable <input type="checkbox"/> Oxygen gas impermeable

3.3 Design Requirements: Standards

This section details the standards and specifications relevant to this project. There are no compulsory standards related to humane care of *C. elegans* due to its classification as an invertebrate. ASTM does have [Guide E2172-01](#) as a standard toxicity test for *C. elegans* toxicity which should be considered as an inclusion in the experimental design. However, there are multiple public online genetic databases such as [wormbook.org](#) which provide guidelines for the maintenance and culture of *C. elegans*. These guidelines were taken into account during the creation of experimental methodologies for this project to ensure that worm health be standardized to the greatest extent possible. Furthermore, experiments using *C. elegans* have employed age synchronization to ensure consistency across all samples with respect to age-related physiology.

The American Society for Testing of Materials (ASTM) provides standard F2150-13 for the testing of hydrogels that will impact the designing of methodology for testing our substrate in which we embed the worm. ASTM F2900 – 11, standards for characterization of hydrogels in regenerative medicine were considered; though regenerative medicine is irrelevant to the scope of this project, considerations pertaining to biological properties and formation kinetics relevant to hydrogel formulation are included with these standards. ASTM F2739, a guide for quantifying cell viability within biomaterial scaffolds, was considered for protocol related to determining successful ability to culture worms in a hydrogel.

The International Standard Organization (ISO) also has standards pertaining to microscopy such as ISO 8036:2015 that will become relevant to operating the neural response monitoring platform. While imaging the designed system, the microscope must be set such that these standards are respected and all materials being imaged do not violate these standards in any way. There are also standards we must adhere to for writing Arduino code. One such standard is the API Style Guide, written by the manufacturers of Arduino, which allows for ease of accessibility for others who wish to collaborate and expand upon the code used in this project. Final standards include

those pertaining to the measurement of light that we will be using for crosslinking the PEG hydrogel and neuronal activation. Ultraviolet radiation can be hazardous to its users - the US department of environmental health and safety (EHS) has safety standards for the safe operation of ultraviolet light sources, which must be considered during crosslinking protocol. Finally, standards from *MicroscopyU* are available regarding the operation and maintenance of fluorescence microscopes, since neuronal imaging is a major part of this project.

3.4 Revised Client Statement

After narrowing the scope of the project and capabilities of the client's lab, the initial client statement was revised to:

“Design a comprehensive research tool that will allow C. elegans to be stretched uniaxially, in order to establish the correlation between neuronal activity and strain.”

3.5 Management Approach

The team selected a Gantt chart (Appendix C) as the primary management tool, presented in a spreadsheet format. The project will be managed on both a whole-project and term-by-term basis with each spreadsheet tab serving as the whole-project or specific term layout. Each tab consists of milestones listed vertically and a horizontal timeline. Block colors indicate the progress of each milestone as “Plan Start,” “Plan Duration,” “Actual Start,” “Actual Duration,” or “Percent Complete.” For financial management, the Gantt Excel file also includes a tab titled “Budget” in which all financial aspects of the project will be closely monitored. This tab consists of a running total of the budget remaining from the school-granted \$1,000.00 USD. Columns are organized such that details of budget items (any costs associated with the design and operation of our system), such as item description, dimensions, number of units, cost, dates ordered and received and expected life with reference to the project timeline are readily and visually available to the team throughout the course of the project.

Table 7: Final Project Budget

Item	Cost
Actuonix PQ-12 linear actuator	\$140.00
2 x PEG hydrogel (1 ml)	\$42.00
37 Agar plates	\$4.81
3 x PFA/FEP polymeric tubing (15 feet)	Free - gifted from Zeus Inc.
Small size zip ties - 2 bags	\$4.00
White, plastic, stickable, square bases - 2 bags	\$2.00
PDMS	\$6.00
Total	\$198.81

Chapter 4: Design Process

The following chapter describes our design process including: a needs analysis for stakeholders, conceptual designs with proof of concept tests, a design constraint assessment, and our initial, alternative, and final design platforms.

4.1 Needs Analysis

After reviewing the client statement, the team hatched a revised client statement as seen in Section 3.4. Through this, the crucial design constraints were classified and used to sort the “needs” from the “wants” in the final design. A “need” is defined as a demand that is necessary for the design of the system. A “want” is an objective that is not necessary but if fulfilled, will be beneficial and complement the final success of the project.

Table 8: Client's Need and Want Considerations

Need:
Design analyzes a single neuron within <i>C. elegans</i> and its reaction to mechanical stimulation
Allows for viewing of the nematode using a light field microscope
Anchor to the substrate of choice consistently
Design incorporates micro actuator to apply a tensile strain of 10% to the nematode
Substrate must not fracture at 10% strain
Must keep nematode alive for 24 hours of observation
Nematode should be immobilized in the x, y, and z planes and within the field of view of the microscope
Uniaxial alignment of worm within substrate
Programmable stroke to produce variable strain/strain rates
Substrates must be optically transparent to allow imaging
Micro actuator needs to apply strain rate of 1 s^{-1} in increments of 10 up to 80 s^{-1}
Apparatus must be submerged in water to prevent mechanical failure of the gel
Want
May be incorporated into a Dual View Inverted Selective Plane Illumination Microscopy (diSPIM system)
Design also enables compressive strains
Design allows strain up to 30%

These “needs” and “wants” will influence product and material selection during design development, and the project’s success will be evaluated by its ability address them.

4.2 Conceptual Design and Feasibility

4.2.1 Conceptual Design



Figure 8: Simple schematic of PDMS stretching apparatus with glued hydrogel embedded with an animal

A single *C. elegans* specimen was embedded within a circular Polyethylene Glycol Diacrylate (PEGDA) hydrogel with a volume of 10 μ L. This was achieved by applying 10 μ L of PEGDA gel solution at a 20wt% concentration on a fluorinated glass slide. These dimensions were just small enough to constrain the worm such that it was visibly conspicuous within the whole gel. PEGDA was selected due to its unique properties of being both highly tunable as far as mechanical characteristics, while maintaining an environment conducive to cell viability. A worm was picked with a flame-sterilized platinum wire and placed within the 10 μ L of gel atop a glass coverslip treated with hydrophobic RainX[®] solution. After one minute of contact to an ice block underneath the slide in order to immobilize the worm and align it uniaxially, the setup was then irradiated with 365 nm ultraviolet radiation for 45 seconds. The worm-containing hydrogel was transferred to a polydimethylsiloxane (PDMS) slab measuring 4.4 x 1.7 x 0.068 cm. One μ L of cyanoacrylate glue was applied to each end of the gel to attach it to the PDMS. PDMS is highly tough and stretchable, making it an ideal material to serve as a stretch transferring medium. A linear actuator driven by a servo motor was used to apply a smooth and controlled strain to the sample from one end, while the other end was fixed. In this particular example, mechanical stimulation took place over an inverted confocal microscope lens under fluorescence, though the apparatus is transferrable to the dimensional constraints of light sheet fluorescence microscopy (LSFM) microscopes as well.

The major advantage of this method for mounting a *C. elegans* sample is that the actuating device will not need to work with small, highly sensitive forces that it otherwise would if the actuator was directly attached to the sensitive hydrogel or to the worm itself, due to the large relative size of the PDMS slab. Additionally, the high elasticity and toughness of PDMS means that large forces applied to it would be translated to a much more subtle force on the hydrogel in the center of the chamber, and ultimately the worm.

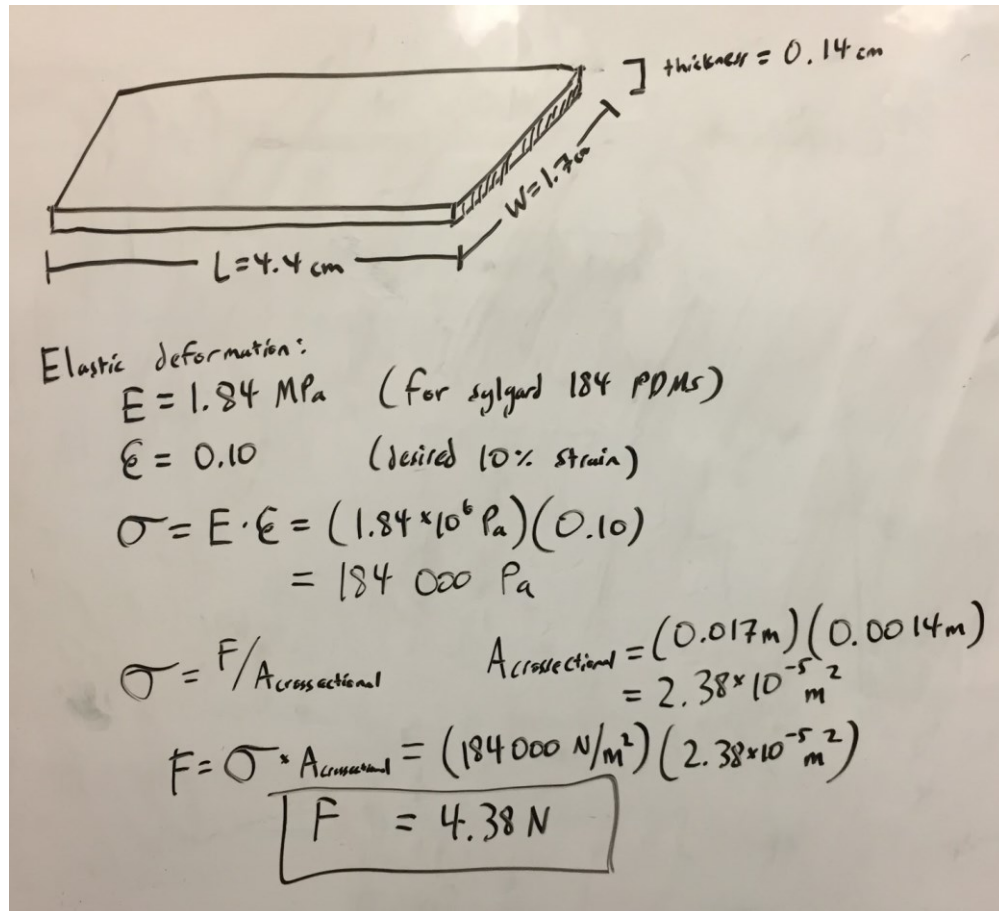
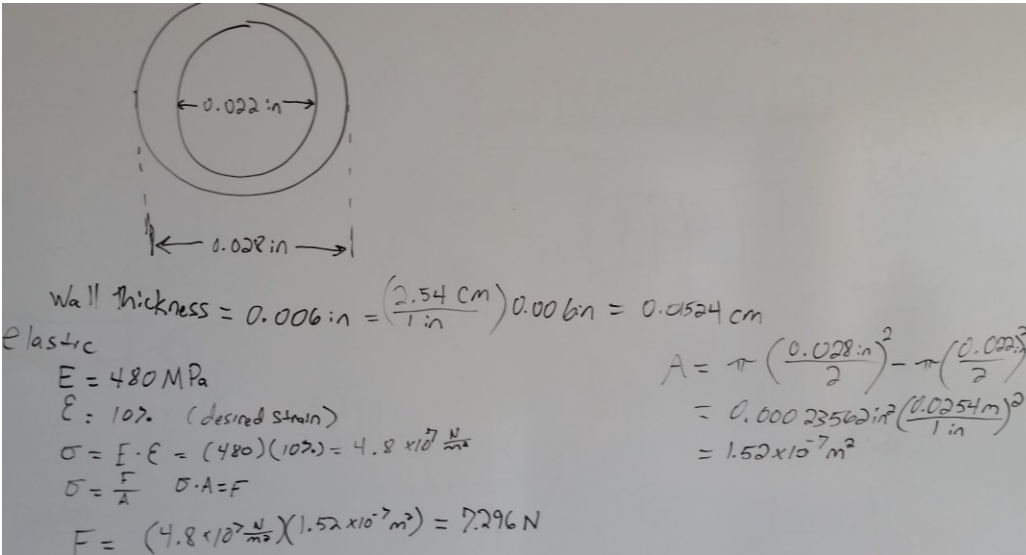


Figure 9 Schematic of uniaxial tensile stress on hydrogel and calculation of approximate force required to induce the required stress to apply a 30% strain on a 4000 Da number average molecular weight PEGDA hydrogel and the worm, assuming uniform behavior between the two.

For the purposes of this schematic, we made a simplifying assumption that the worm will stretch at the same level and rate as the hydrogel, and that the hydrogel would be adhered to the PDMS well enough that it would stretch along with it. This was a necessary assumption to make since there is no publically available data pertaining to stretching worms in a PEGDA hydrogel,

and we would have to characterize this relationship ourselves. If a difference is observed between worm and gel strain during initial experimentation, a data set correlating the strains and strain rates will be created with the intent of creating a correlation curve, so that the actuator load to be applied can be calculated based upon the desired worm strain and strain rate.

Alternatively, a small-diameter tubing could be used to house the gel and worm. Here, the force needed to stretch the materials to the desired stretch parameters would follow the same calculation from Figure 8 with a modified cross-sectional area, as shown in the calculation below, as well as appropriate Young's Moduli when using materials different from PDMS. These calculations were validated with 5N actuator, since we had already purchased that actuator when the polymeric tubing concept came about. The actuator was indeed able to stretch PFA tubing to 10% strain, albeit with resistance - likely a result of the actuator operating slightly above its rated force limit.



$\text{Wall thickness} = 0.006 \text{ in} = \left(\frac{2.54 \text{ cm}}{1 \text{ in}}\right) 0.006 \text{ in} = 0.01524 \text{ cm}$

$E = 480 \text{ MPa}$

$\epsilon = 10\% \text{ (desired strain)}$

$\sigma = E \cdot \epsilon = (480)(10\%) = 4.8 \times 10^7 \frac{\text{N}}{\text{m}^2}$

$\sigma = \frac{F}{A} \quad \sigma \cdot A = F$

$F = (4.8 \times 10^7 \frac{\text{N}}{\text{m}^2}) (1.52 \times 10^{-7} \text{ m}^2) = 7.296 \text{ N}$

$A = \pi \left(\frac{0.028 \text{ in}}{2}\right)^2 - \pi \left(\frac{0.022 \text{ in}}{2}\right)^2$

$= 0.00023562 \text{ in}^2 \left(\frac{0.0254 \text{ m}}{1 \text{ in}}\right)^2$

$= 1.52 \times 10^{-7} \text{ m}^2$

Figure 10: Cross sectional area calculation for tubing design (OD = outer diameter, ID = inner diameter)

$$A_0 = \pi \left(\frac{OD}{2}\right)^2 - \pi \left(\frac{ID}{2}\right)^2$$

4.2.2 Feasibility

This next section outlines tests to assess the feasibility of the various design components and key questions that these tests will answer. One question that arose was the actuator's ability to strain the hydrogel up to 10% of its original length. This goal seeks to replicate the 10% neuronal strain that can be experienced in a TBI event. If we can stretch the hydrogel, we must also confirm that the hydrogel is interacting with the model organism properly to provide optimal test conditions as well as facilitate imaging.

4.2.2.1 Substrate Testing

- a. *Can the hydrogel strain up to 10% of its original length?* (Addressed in 4.2.2.3)
 - i. Will the gel itself remain intact and within the elastic deformation region?
 - ii. Will the clamping system hold onto the gel and translate stress via gel markers and external visual cues?
- b. *Will *C. elegans* interact properly with it?* (Addressed in 4.2.2.3)
 - i. Can the worm be aligned and stay uniaxially along the length of the gel?
 1. Cool the embedded substrate to ensure alignment
 - ii. Will the worm stretch accordingly with the gel in a predictable relationship?
 1. Does the organism maintain biomechanical functions throughout strain?
 - iii. Can the worm remain viable in lab-synthesized substrate?
 1. Can effects of biochemical processes be seen on the functionality of the organism?

4.2.2.2 Actuation Apparatus Testing

- a. *Can it consistently apply tensile strain and strain rates to the required parameters?*
 - i. Up to 10% strain to substrate of known dimensions, requiring appropriate force
(See Figures 9 & 10 for calculations)
- b. *Can it consistently and reliably clamp onto the gel?*
- c. *Will it fit within the dimensional constraints of an appropriate imaging platform?*

4.2.2.3 Initial Feasibility Testing Results

Initial feasibility testing indicated that the worm will stretch with the substrate. Animals were mounted according to the procedure outlined above. Initial tests of stretching the PDMS with an empty 20wt% PEGDA hydrogel indicated that PDMS could be stretched up to 10% before hydrogel fracture. Further trials with embedding whole-brain imaging worms [42] allowed measurement of head-to-tail distance pre-and post-stretch under a rhodamine filter, using ImageJ line measuring tool. Across three trials, maximum worm strain achievable before gel fracture averaged 10.33%, with a standard error of +/- 0.81%. This outcome is solely indicative of the fact that the PEGDA substrate grips the worm strongly enough to stretch the whole organism. However, due to insufficient resolution of neuronal nuclei, it could not be determined with reliability whether the neurons stretched with the worm in this specific test. Though tests were not performed to determine the maximum stretch of the gel before failure, it can be assumed that it stretched 10% due to strong adherence between the gel and PDMS slab due to strong cyanoacrylate glue adherence. Detailed feasibility testing data can be found in Chapter 5.

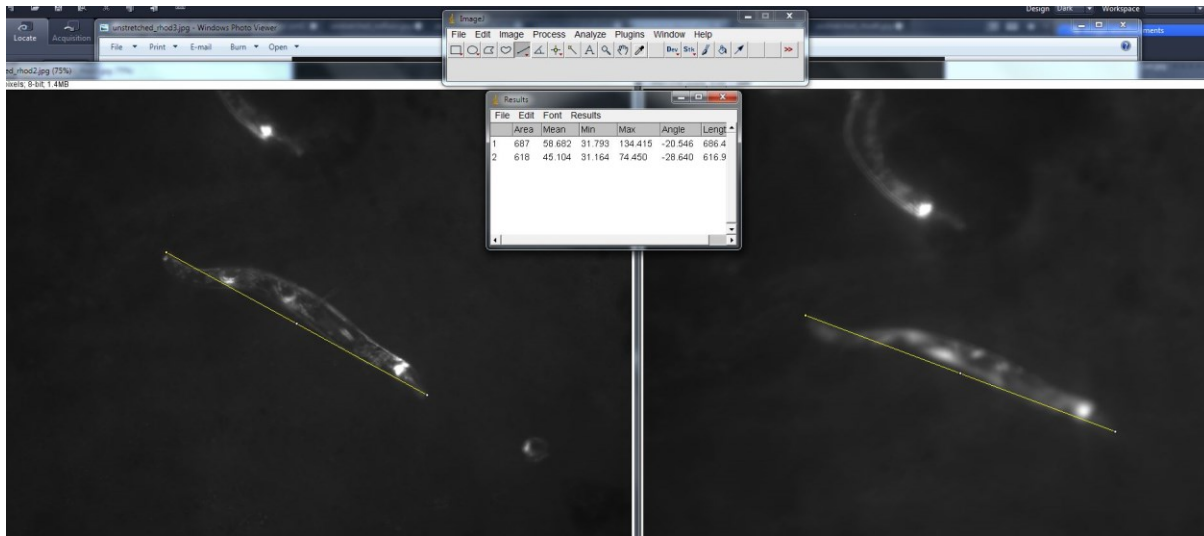


Figure 11: Images and strain results (performed in ImageJ®) for a stretch trial with the superglue and PDMS based apparatus

4.3 Alternative Designs

The alternative designs consisted of three distinct parameters that were distinguished based upon logistics, feasibility, and relevance to the fields of interest. A limiting factor in the design selection phase for each parameter was time; some methods were not feasible because they fell outside the scope of our timeline. Similarly, some methods were not pursued because they required materials or expertise that we could not obtain or master. The financial limitations are strictly imposed by the budget within the project, as there are no existing competitors on the market. The three alternative design parameters were: the actuation device, the substrate mounting platform and the imaging system. The following section details alternatives for each of the three design parameters.

4.3.1 Alternative Designs for Actuation Device

Two techniques were considered for fixating the stretching apparatus while mechanically straining the worm. First, we characterized the stretch as uniaxial tension. We created an anchor

point on one side of the PDMS housing and attached an actuator to the unanchored side of the housing. This allows us to use only one actuator and is more cost effective. The other design is to attach two actuators that will pull in opposite directions simultaneously. This would induce a similar strain to the single actuator with an anchor point but may stretch the worm within the housing more effectively. This technique may keep the worm within the 3 mm by 3 mm field of vision of the microscope more effectively than the anchored technique. It may also allow us to achieve faster strain rates than the anchored design. However, coordinating both actuators to simultaneous and identical stretches introduces added difficulty to the apparatus' implementation. Our initial, alternative, and final designs all utilized the first fixation technique i.e. one actuating side and one fixating side.

4.3.2 Alternative Substrate Designs

The substrate for these designs are all a PEGDA hydrogel that encapsulates the worm because of its desired biocompatibility and photocrosslinking ability. The variable is the technique in which the worm-embedded gel is housed and stretched.

4.3.2.1 Silane Glass Cover Slip

Silane methacrylate is a chemical agent which can be used to treat a glass surface such that PEG-diacrylate will bind covalently to it. The silane methacrylate is used to treat a glass surface such that it binds to it. The methacrylate groups, facing up from the glass, can then covalently bind to the diacrylate group in the PEGDA gel solution upon UV irradiation [43]. This covalent bond is much stronger than the weak interactions that occur between the hydrogel droplet and the glass without silane treatment. This attribute is useful for mounting the hydrogel to the PDMS platform.

This technique requires the use of two glass microscope slide coverslips that will serve as the anchor points. The ultimate goal of this design is to achieve an orientation that allows the hydrogel to be a free floating structure between two opposing coverslips that will then be attached to the PDMS for stretching. When a uniaxial load is applied to the hydrogel in between these anchor points, the tensile force translates from the PDMS through the hydrogel.

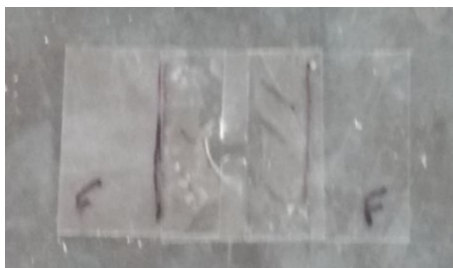


Figure 12: Silane treated coverslips as anchor points with a third coverslip as a cover prepared for crosslinking

The advantage of this design is that the materials used are commonly found in laboratories. Another advantage of silane is the ease of application. The silane treatment on the glass is manageable to custom areas of the glass coverslip due to the viscosity and hydrophilicity of the silane. This makes it possible to spread the silane with the use of a pipette tip to distribute in the necessary manner across the glass. It is then possible to mark treated and untreated areas within the same glass coverslip. The gel is also strongly bonded with the glass in this interaction, resulting in a failing stress that is solely dependent on the ultimate tensile strength of the hydrogel rather than the failing strength of the anchoring points. This is ideal for reducing failure variability.

The disadvantage of this design is only seen in carrying out its preparation. The hydrophilic nature of silane that makes it manageable for covering the glass coverslip also causes the hydrogel to wick (move) into spaces, through unavoidable capillary action. Its hydrophilicity is the key to the covalent bonding of the hydrogel to the glass, which is why treating the silane coverslip with

a secondary treatment of a hydrophobic solution (Rain X®), has a prohibitory effect resulting in an incomplete bonding between hydrogel and coverslip.

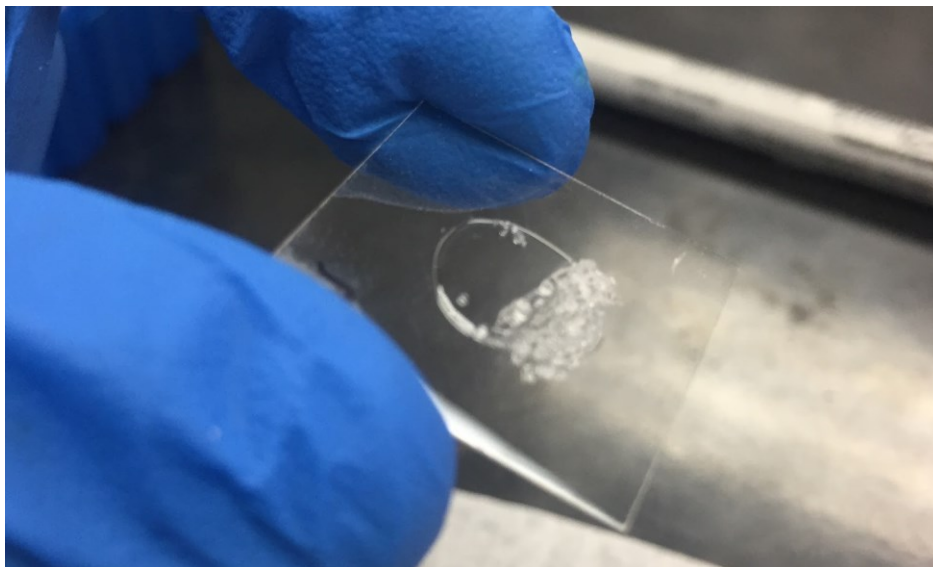


Figure 13: Proof of the strength of silane treated coverslip bonding to hydrogel



Figure 14: Image of PDMS slab with a hydration well

4.3.2.2 PDMS Slab with Hydration Well

Figure 14 shows the alternative design of the PDMS block with a well in the middle. The purpose of this design is to provide a large and flexible platform (PDMS slab) with which to grip onto. The well served to allow the hydrogel to remain submerged in water while being imaged because the hydrogel loses its normal mechanical properties when dehydrated. The trade-off here was that the larger, more manageable PDMS slab must be attached to the small and fragile hydrogel that contains the nematode. The PDMS was flexible enough to transfer strain to the hydrogel when the hydrogel is stretched. The PDMS was created with about 16 g of PDMS gel in a standard weight boat. The well was created when a coin was placed into the bottom of the gel before the PDMS was vacuumed and cured. The PDMS slab was gripped by binder clips to transfer the strain from the linear actuator to the gel as seen in Figure 13.



Figure 15: PDMS slab with gripping binder clips to attach to linear actuator

The hydration well successfully holds water after the hydrogel has been attached to the bottom. This can be used in substitute of the well that exists in the diSPIM. This serves to keep the gel hydrated and works with the objective lenses that must be submerged on diSPIM.



Figure 16: PDMS with hydrogel successfully attached and hydration well filled

Silicone is often used as a platform to seed biological cultures because of its high biocompatibility. The material's elasticity marks it as an excellent choice of material for applying cyclic tensile strains, as seen by its wide use in mechanobiological studies [51]. Because of these material properties, silicone serves as a viable alternative substrate material in which to imbed a worm and apply a stretch.

4.3.2.3 Tubing with Hydrogel

The team cut a 5 mm section of cylindrical Masterflex Tygon® silicone tubing of 2mm inner diameter (ID) and filled a section of it with 50 μ L DI water. Upon physical stretch by hand, the tubing appears to stretch sufficiently up to over 10% strain without issue. A worm was then seeded into the water, and laid horizontally over the inverted objective of a Zeiss Axiovert 40 CFL scope. Capillary action of the tubing prevented water and worm from flowing out of the tubing even when laying horizontally. A wooden stirrer was split in half and set down on either side of the scope's objective in the x-y plane for improved image resolution and to ensure that the small

section of tubing would not fall through the gap in the scope stage. The following image was obtained while pinning the tubing down to the wooden stick supports on either side of the objective:

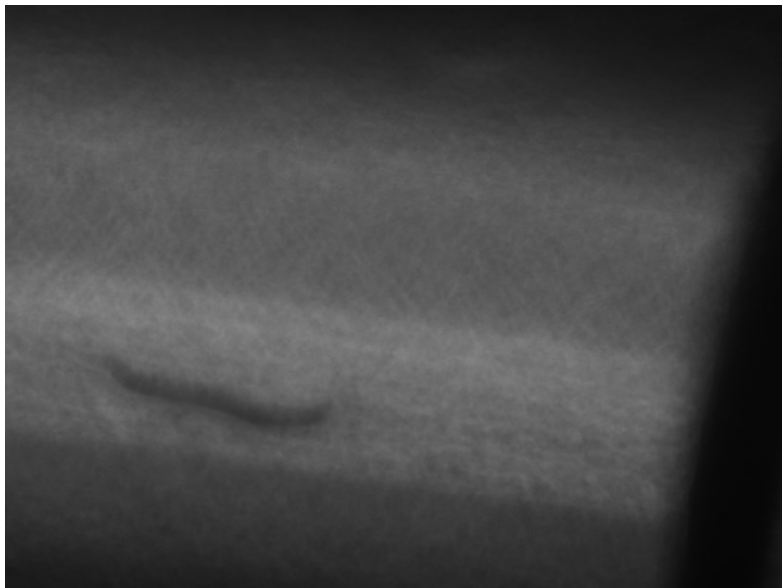


Figure 17: Worm imbedded in 2 mm ID silicone tubing

The worm was visibly swimming in the solution within the tubing, indicating its viability. Next, the rhodamine fluorescence filter was applied, producing the following image:

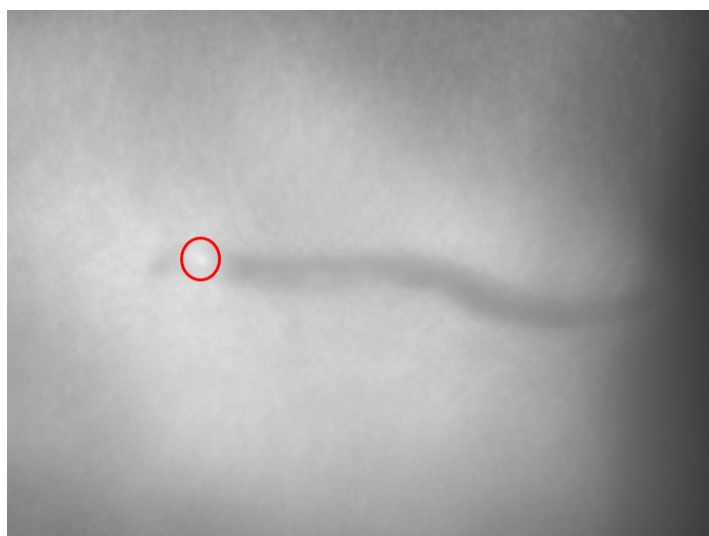


Figure 18: Worm imbedded in 2 mm ID silicone tubing showing fluorescence under non-ideal conditions

The small white section of the worm indicated by the red circle indicates a cellular nuclei illuminated by the rhodamine filter. However, image focus and resolution must be improved to confirm this with more certainty. These initial results identify this design as a viable alternative but there are also ways in which this design can be improved, and more tests need to be done in order to further validate it.

The team also has 1 mm inner diameter tubing available with which to try this test, which may facilitate focusing on the worm at higher magnification and elongating uniaxially with the tubing. Other tubing materials with improved optical clarity can be assessed. In order to improve the image focus, the DI water could be replaced with the PEGDA hydrogel which would be photocrosslinked within the section of tubing. Previous experiments have already confirmed image clarity while using the PEGDA gel.

4.3.3 Alternative Designs for Imaging Platform

The imaging platform is the third and final principal component of the system design. This component encompasses how neural activity will be monitored, including biochemical markers and the microscope. The client, Prof. Albrecht, proposes using a wide-field confocal microscope because of its availability in his lab and his prior experience validating its use in microfluidic devices using PDMS housings [20]. One advantage of wide-field confocal microscopy is that it allows us to study correlations in neuronal activity of the entire animal [44].

Although the client has already specified the imaging platform and marking technique to be used, it is still important to consider alternative ways in which the worms could be monitored and imaged. Firstly, it has already been established that a potential goal (“want-to-have” feature) of the devised system is to make it compatible with diSPIM. Achieving this alternative is facilitated by the fact that Prof. Albrecht plans to implement the diSPIM using a stage with similar dimensions

to a confocal microscope (i.e. the dimensions of the apparatus would not have to change). However, the substrate content may have to be altered in order to achieve the necessary optical properties such as refractive index for adequate imaging of the modified diSPIM.

A second alternative is to change the mechanism of neuronal activity monitoring. Despite the client proposing the use of fluorescent marking of calcium channel activity, electrophysiological measurements are a more direct way of quantifying neuronal activity. For *C. elegans*, this entails attaching microscopic electrodes to the organism. The stretching of the substrate and the worm will introduce a high level of physical instability and electrical noise to hypersensitive microelectrodes, thus electrophysiological means of neuronal monitoring are impractical for this project. Because of its ease of use, optogenetics has become the “gold standard” for measuring neuronal response. This works on the principle of a genetically engineered *C. elegans* strain that expresses a GCaMP that will increase in fluorescence when bound to calcium. This fluorescence is then measured quantifiably through the use of imaging software that reads the output of the fluorescence microscope.

4.4 Final Design Selection

Ideally, our final design would produce a reproducible platform that ensures feasibility for the user’s experiments and reliable results. Data collection is a key component in the advancement of TBI research and our project. For this reason, we elected to pick a final design that would enhance the process of collecting strain data. The major constraints taken into account were time, feasibility, reproducibility, available imaging platform, and strain data.

4.4.1 Final Design Considerations, Tubing vs. PDMS

Our initial design utilizing PDMS was enhanced several times. First we used tape to secure the hydrogel to the PDMS, then silane treatment, but lastly we found cyanoacrylate glue to work

best. Each improvement to the PDMS method was a step in the right direction, but also brought up novel, unforeseen problems. For example, the PDMS with the hydration well design was introduced to solve the problem of keeping the gel hydrated during imaging. However, this design brought about a variety of challenges including imaging at different depths and fixation in a hydrated well. Any given PDMS stretch trial took approximately one to two hours and rarely were we able to obtain desired data and images. After several attempts to create a reproducible lab protocol via the PDMS method, we decided to simultaneously pursue alternative design options.

The client Prof. Albrecht suggested utilizing miniature, transparent, stretchable, and oxygen-impermeable tubing as a platform for stretching. The advantages of using tubing opposed to a PDMS slab are:

- ❖ Enhanced fixation (for the tube itself and for the hydrogel inside the tube)
- ❖ feasibility in embedding and crosslinking *C. elegans*
- ❖ Hydrogel structure and maintenance i.e. hydration, and reproducibility.

A decision matrix below with six categories compares the two leading designs quantifiably in order to select the optimal design apparatus moving forward. Points are assigned to each material on a scale of ten.

Table 9: PDMS versus Silicone Tubing Design Decision Matrix

	PDMS	Polymeric Tubing
<i>Imaging</i>	7/10: PDMS itself producing imaging through, but difficult to keep worm in field of view	5/10: Tubing allows imaging through itself, difficult to keep focus on worm and in field of view
<i>Stretchability</i>	9/10: Stretchable and durable, possible to obtain multiple trials on one slab if no stress concentrations or fractures occur	7/10: Highly stretchable but only one trial is possible per tubing section
<i>Material Fixation to Actuator During Stretch Trial</i>	7/10: Obtained strain data with images from stretch trials of PDMS slab alone	8/10: Obtained strain data from stretch trials of tube alone, easy to attach to actuator, slight slippage on both sides can be improved upon
<i>Hydrogel Fixation to Material</i>	3/10: Tested several designs but still struggle with translating stretch from PDMS to hydrogel i.e. embedded worm	9/10: Hydrogel crosslinks perfectly inside tube, can verify by pushing syringe down fully (resistance can be felt if properly crosslinked), worm-stretch translation data can be seen
<i>Lab Protocol Feasibility</i>	1/10: Too many variables, extremely difficult for user to obtain strain data	7/10: Details are confusing and setup is intricate, but works for accustomed users
<i>Reproducibility</i>	3/10: Extremely difficult to obtain precise results for multiple stretch trials	6/10: Stretch trials have been consistent, lab protocol is easy to follow and implement
Total	30/60 = 50%	42/60 = 70%

After several months of trials and a quantifiable matrix analysis of both designs, it was evident that the polymeric tubing was the favorable design for stretching purposes.

4.4.2 Final Design Specifications

4.4.2.1 Tubing

The first step in creating a silicone tubing stretching apparatus was to create a list of design criteria for tube selection. This criteria constituted the design constraints to allow stretch trials (with an embedded worm) to be completed. The following constraints guided us in the search for silicone tubing: high elasticity, optical and UV transparency, oxygen gas impermeability, and miniature diameter.

Firstly, the tubing must be stretchable to allow collecting strain data on *C. elegans*. Elastic tubing allows multiple trials to be performed on any given section of the tubing. Optical and UV transparency are important for the premise of our research because these properties allow specimen imaging to be performed on confocal and fluorescence light sheet microscopes. Specimen images through our selected tubing via either confocal or fluorescence microscopes can be found in Appendix. Oxygen impermeability is a key factor that allows consistent hydrogel crosslinking to occur. If UV light is introduced to the PEG hydrogel in the presence of oxygen, the oxygen scavenges free radicals to the structure preventing the crosslinking mechanism from working. This problem is why the PDMS method scored poorly in Table 9 above; the hydrogel rarely fully crosslinked on the microscope slide even with a cover slide on top. Oxygen impermeable tubing is a necessity and the solution to our hydrogel crosslinking challenges. The last tubing constraint is its size which includes its length and diameter. The tubing must have a diameter small enough to encapsulate the worm in the uniaxial direction, but should not be big enough for the worm to move freely in the width direction. This minimizes the worm's positioning variance from trial to trial. Also, a small tube diameter decreases the volume of hydrogel needed each trial.

Given the constraints listed above, we contacted Zeus®, a tubing manufacturer, and they recommended three types of fluoropolymer tubing: FEP and PFA (detailed in section 2.4.3). The

manufacturer offered to send 15 feet of two different FEP tubes and 15 feet of a PFA tube. The nominal inner diameters of the tubing are 0.018 in (FEP 26 gauge) and 0.022 in (FEP 24 gauge, PFA 24 gauge).

4.4.2.2 Actuator

Precision and repeatability are the other two major constraints that were considered when selecting an actuator. After the team surveyed the market for devices according to the constraints outlined in Section 3.2.1.1 market research, we selected the Actuonix® PQ12 actuator which has a stroke length of 20 mm, a maximum speed of 28 mm/s, a maximum force of 5 N and a positional repeatability of ± 0.1 mm. A 5N actuator was purchased on the premise that the PDMS slab method would be employed. However, with the conception of the tubing method after obtaining the actuator, the requirement to stretch polymeric tubing sufficiently increased to 7N. We tested and found that our actuator could stretch the tougher polymeric tubing sufficiently, albeit at a slower rate than optimal. Despite suboptimal force parameters, this actuator meets the design constraints of providing a suitable, cost effective proof-of-concept for easily programmable stretching while conforming to the spatial constraints of actuating over a microscope objective. It is limited in that the magnitude and rate of force it can induce cannot be controlled. Higher end models with similar programmability but more controllable force and retraction rates can be considered for future iterations of our proof-of-concept.

Tube attachment to the Actuonix® is achieved by directly weaving and tying one end of the tube through the actuator arm and securing it in place with cotter pins. The other side of tubing is threaded through a mounting base and fastened with zip ties. The mounting base can be stuck directly to the microscope platform surface and the actuator can attach to the side of the microscope with a command hook. This design can be enhanced using stronger and more durable materials

than our current design which consists of a plastic mounting base, plastic zip ties, a command strip, and cotter pins.

Chapter 5: Design Verification

This chapter presents the numerous tests conducted to verify the final design, including individual components and the entire ensemble. It also addresses how the results relate to the established objectives.

5.1 Tubing Material Selection

Summarizing the design specifications, the polymeric tubing must be:

Table 10: Polymeric Tubing Design Specifications

<u>Specification:</u>	<u>Rationale:</u>
1. Small diameter < 0.56mm	Workable size with microscopic worm
2. Optically transparent	Enables imaging of worm and neuron through tubing
3. UV transparent	Permits UV irradiation to crosslink PEG hydrogel
4. Oxygen gas impermeable	Prevents oxygen gas inhibition during crosslinking
5. Stretchable up to 10%	Translate stretch to neuron

The fulfillment of these requirements was assessed through multiple tests. First, the photocrosslinking ability of PEG within both FEP and PFA tubing samples was verified by injecting 5 μ L of 20wt% PEGDA solution into a 5 cm section of tubing, and irradiating with 312 nm UV light for 45 s. Applying suction with a syringe to the crosslinked gel segment did not displace the gel, verifying that it had thoroughly crosslinked within the tubing. Furthermore, worms were incorporated into the setup to verify their immobilization in this setup (Figure 17), which was confirmed again using a syringe.

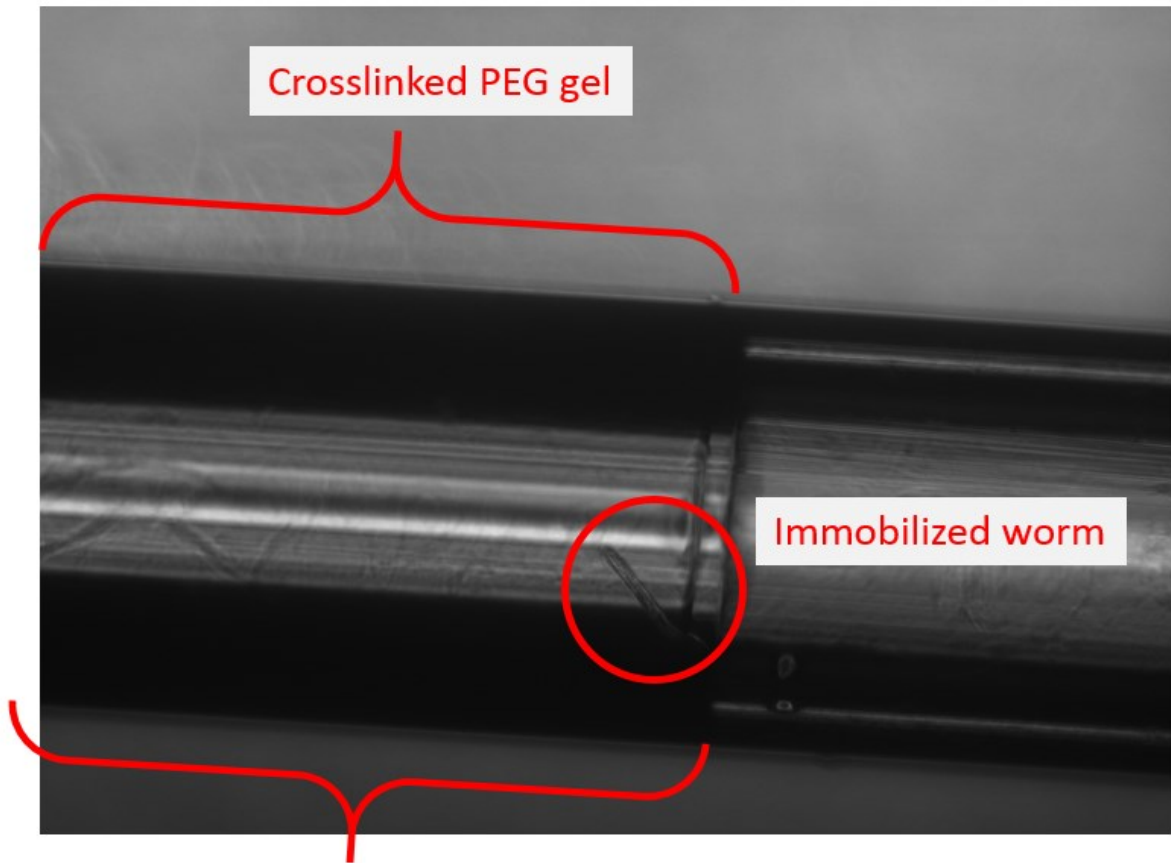


Figure 19: Immobilized worm within a photocrosslinked PEG segment in PFA tubing

Next, the strain response properties of each tubing material were compared quantitatively in order to select one of the two as the optimal tubing material for the final design. This was accomplished by putting multiple samples of PFA and FEP under multiple strain cycles.

Three zip ties, two parallel and one normal to the tubing axis, pinched the tube tightly to the 1" x 1" square adhesive base on the fixed end. On the stretched end, tubing was wrapped around and pinched by a small cotter pin and fed through a hole in the actuator arm. Strong adhesives secured the actuator body to the benchtop. The actuator arm's initial position was at full extension (0% stroke).

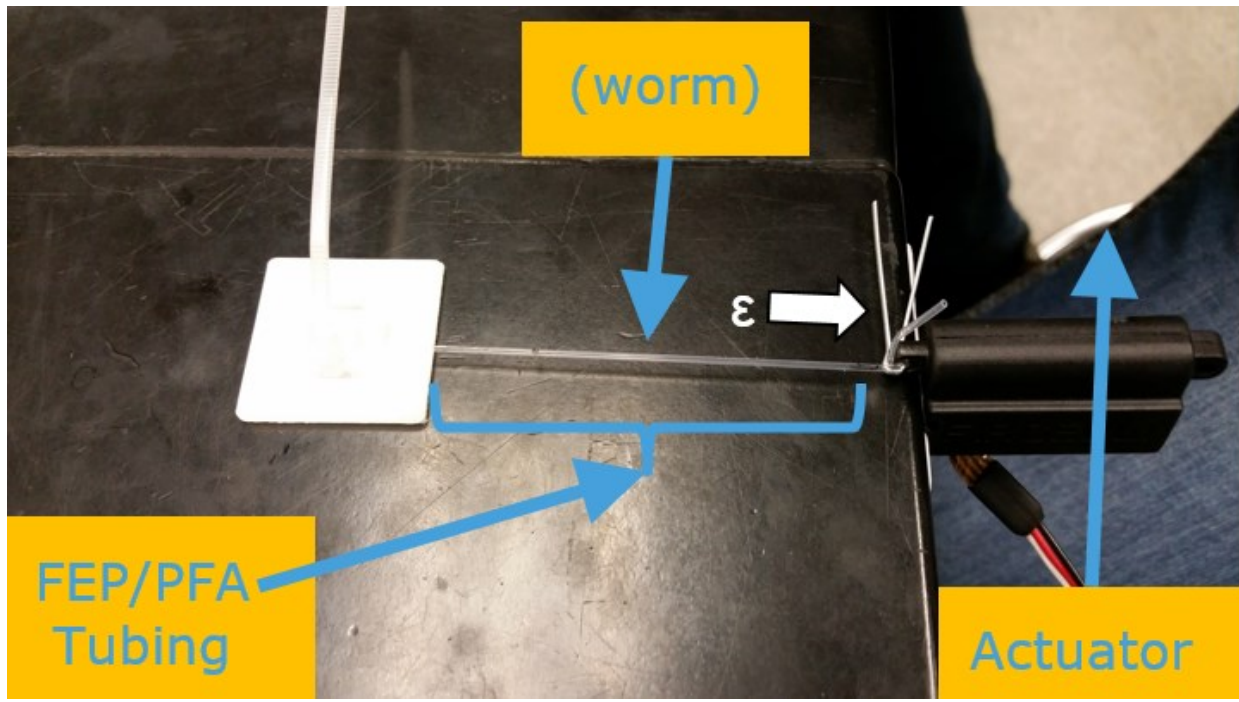


Figure 20: Setup for the tube stretch tests with fixed end (left) and stretch end (right)

Two 8 cm samples each of FEP and PFA underwent three strain cycles (N) with strains increasing from 0-100% of the Actixon PQ12® arm length (28 mm) in 10% increments. The second FEP sample additionally underwent a fourth strain cycle.

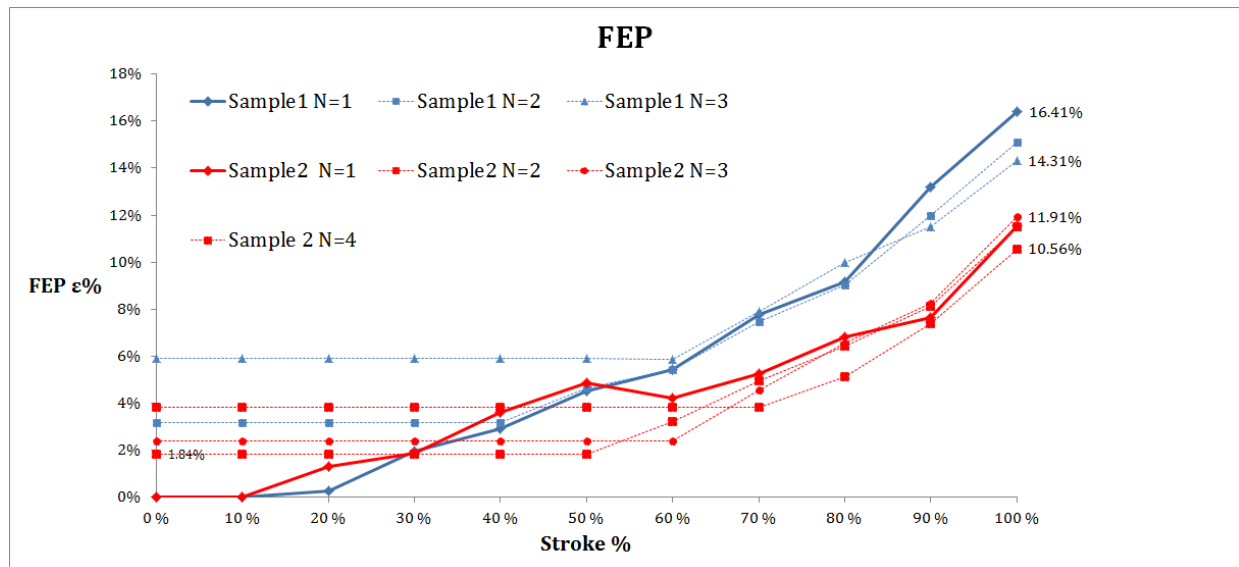


Figure 21: FEP Stretch Results

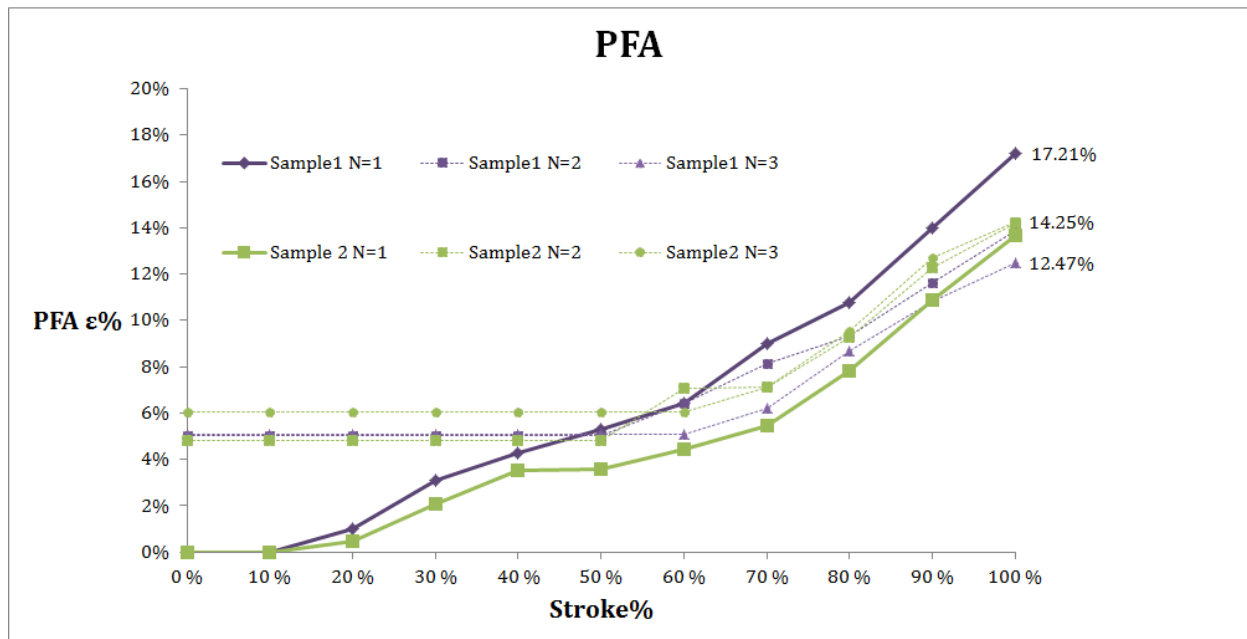


Figure 22: PFA stretch results

The FEP samples achieved maximum strains of 16.41% and 11.55% of their original length at 100% stroke length on the first cycle, while the PFA samples strained maximally at 17.21% and 13.66%. Once the actuator arm returned to 0% stroke position, noticeable slack was present due to the initial stretch, requiring a higher stroke % position as a nominal strain. For the FEP samples, the starting position varied from 40-70% stroke on the second, third and fourth cycles. These cycles produced variable maximal strains ranging from 6.50-11.55%. The PFA samples, on the other hand, had more consistent starting positions at either 50% or 60% stroke, achieving maximal strains within a narrower range of 7.05-8.96%.

These results indicated plastic deformation after the first stretch cycle. Additional cycles would therefore require recalibrating the tubing by pulling the extra tubing slack through the base and measured for strain before initiating a second stretch cycle, which would interrupt workflow for neural response testing. For this reason, the strain properties on solely the first stretch are weighted more heavily for selecting the optimal tubing material.

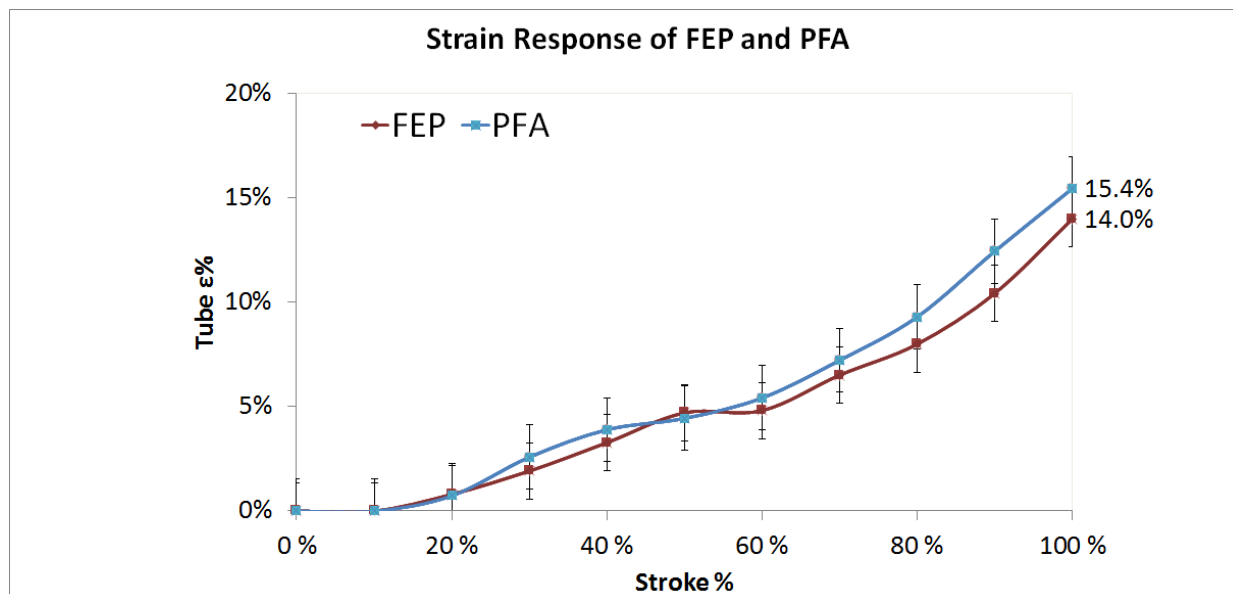


Figure 23: FEP and PFA Strain Response

PFA achieved average maximal strain of 15.4% at 100% stroke, while FEP achieved 14.0%. These results are not statistically significant with a p-value = 0.143, hence the final tubing material choice must be made based on the criteria of optical transparency for optimal image quality. PFA has a better optical transparency [45], and was thus selected as the tubing material of choice for the final design.

5.2 Worm Strain

On February 28th of 2017, the first series of tubing stretch tests with worms over fluorescence imaging was conducted in the lab. A group of whole-brain imaging worms were individually picked and crosslinked into 5 μ L of 20 wt% PEGDA hydrogel within a segment of FEP tubing. As in previous tests of tubing material properties, an adhesive square base plate was

attached to the microscope stage and used as a fixed end for the tubing. On the other end, the tubing was attached to the actuator using a cotter pin (see previous Figure 23).

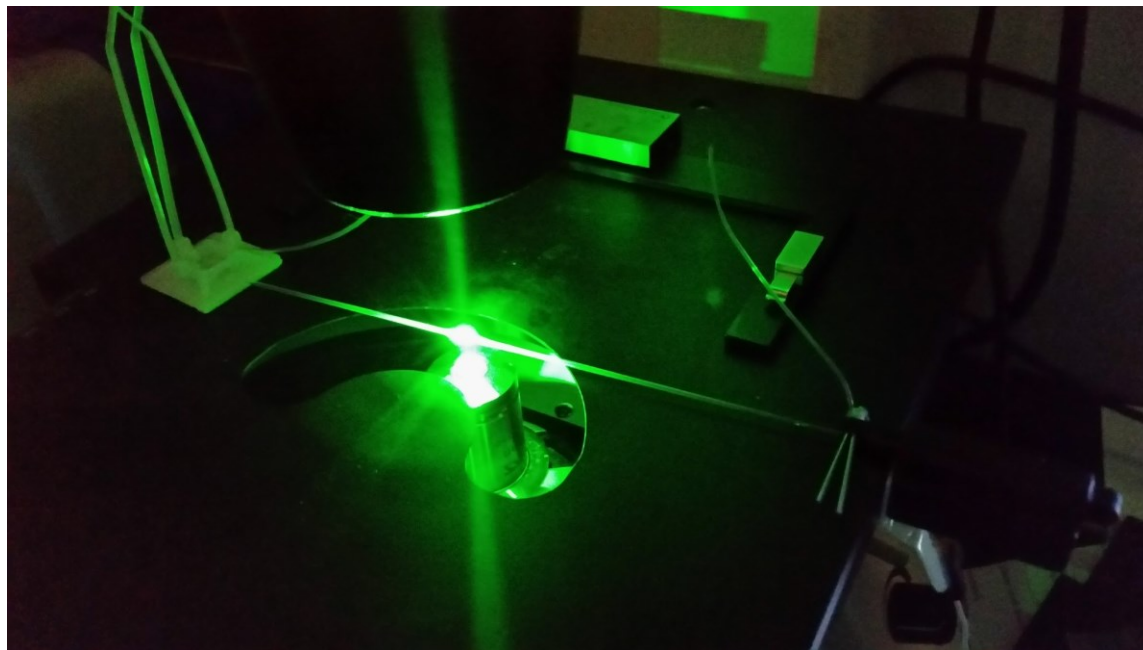


Figure 24: Tube stretching setup over rhodamine fluorescence

Worm nuclei were successfully illuminated under rhodamine irradiation (Figure 24), with multiple animals being localized in a small segment of gel. Fine adjustment on the microscope focus allows different worms to be in focus due to their localization in three dimensional space.

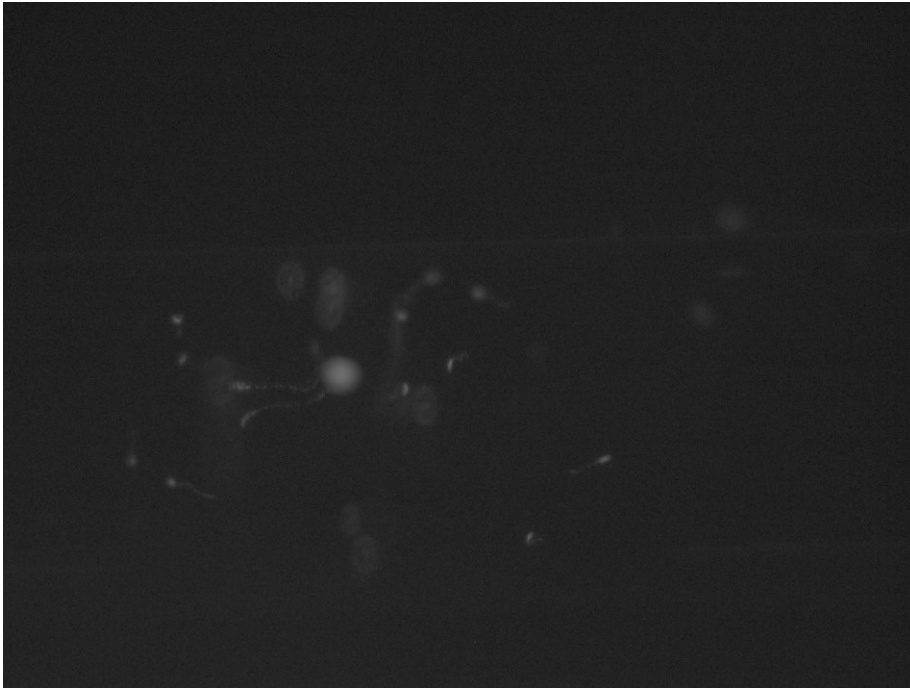


Figure 25: A series of whole-brain imaging worms under Rhodamine fluorescence during a stretch trial in FEP tubing

One worm was selected, and reference points (head and tail) were selected on each end of the worm to use as strain markers. Stress was applied to the tube in increments equivalent to 10% of the actuator's stroke length. In many cases, the actuator would have to be started at 50% stroke due to slack in the tubing. Trials ended at 80% stroke because, beyond that, the selected worm would move outside of the camera's field of view. For three separate trials, the change in worm length was measured in pixels through ImageJ in stroke ranges from 50-80% (Figure 26, Table 11), achieving an average maximum worm strain of 2.9%. In tube stretch verification trials, the tube strain also increased by about 3% in the stroke range of 50-80%. Based on the equivalent strains obtained from the worm and tubing over the same actuator arm range, we were able to conclude that the worm embedded in hydrogel will stretch approximately the same amount as the encapsulating polymeric tubing. Ideally, range of data wider than the 50-80% window could be obtained with a wider field of vision from the microscope camera so the stroke can go over 80%, and with better control of tubing slack in the initial setup so stretching can begin below 50% stroke.

This would allow for more conclusive data regarding the equivalence of worm and tubing stretch to be generated as a key design verification.

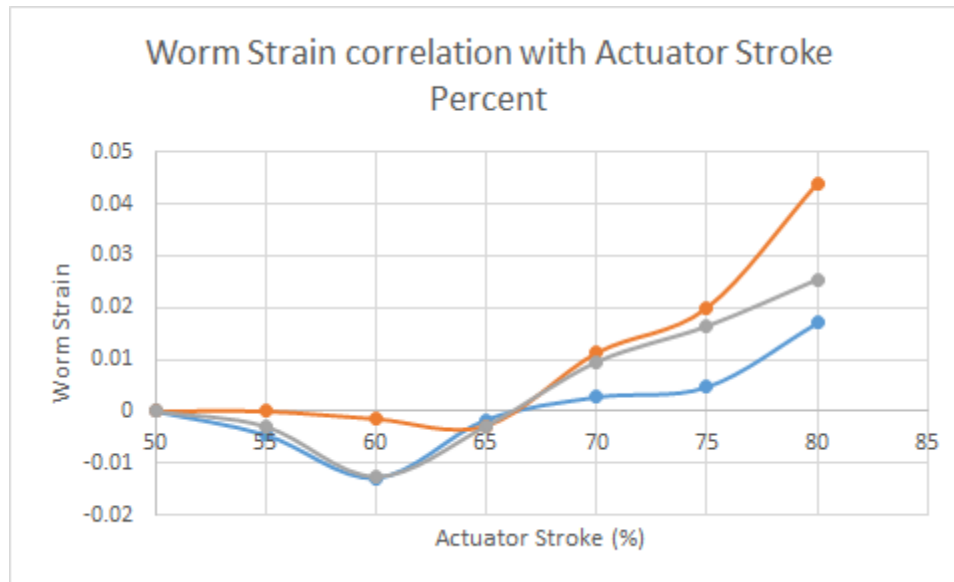


Figure 26: Three separate trials of tubing stretch correlate with worm strain as measured by pixel count changes in ImageJ®

Table 11: Maximum Strain for each trial

Trial	Worm Strain (%)
1	1.7%
2	4.4%
3	2.5%
Average	2.9%

5.3 Frame

Initially, tubing with embedded animals was placed over the microscope objective using the setup shown in Figure 27 (strain test). This approach produced poor image resolution due to large working distance from the scope's objective, and the inevitably fixed setup to the microscope stage. This revealed the necessity for a frame onto which the actuator could be attached and the

tubing directly secured. This effectively allows for transfer between scopes, including a diSPIM platform. A frame piece (Figure 27) was designed initially to be 3-D printed.

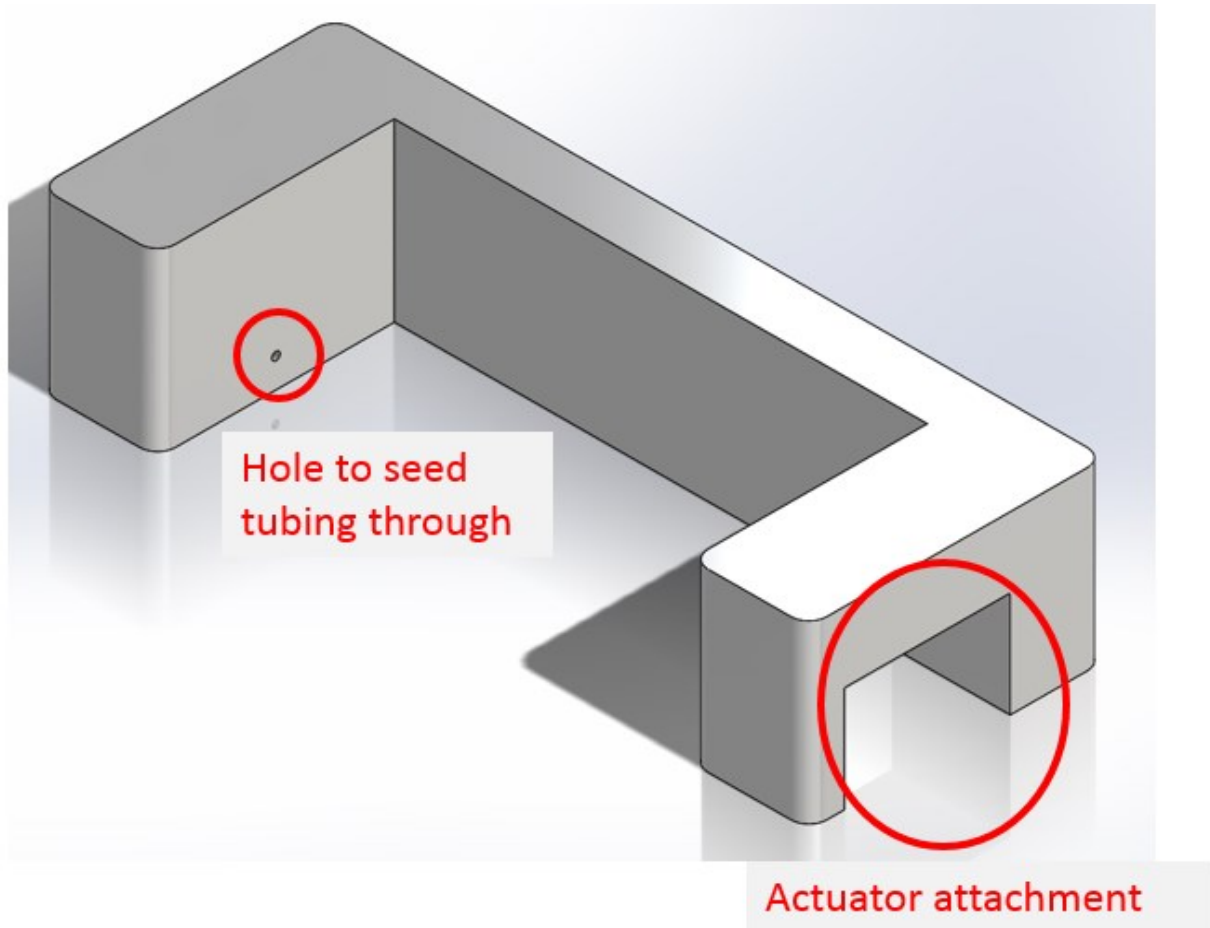


Figure 27: Initial Frame Prototype

This initial prototype could be produced easily using a rigid acrylonitrile butadiene styrene (ABS) polymer at a low cost of \$9.96 per model. However, this design does not account for the tubing fixation at both ends of the frame. The tubing end on the hole side would be able to move freely through the hole, in turn preventing it, and the worm from stretching. The implementation of a hex bolt on this side addresses this need, but drilling threaded holes into ABS material proved to be problematic. As a result, the design was modified to incorporate this securing mechanism.

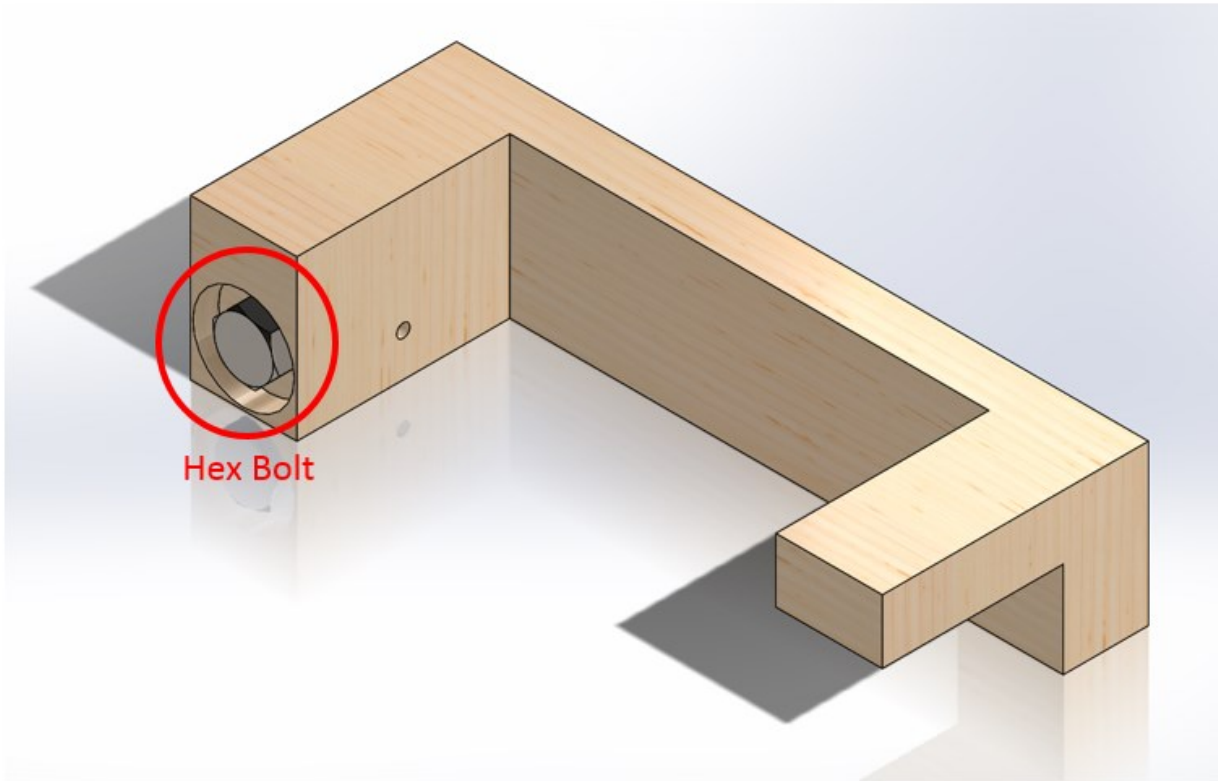


Figure 28: Modified frame prototype

Furthermore, we found that this modified prototype could be manufactured more easily and at an even lower cost by laser-cutting several layers of maple wood and stacking them using cyanoacrylate glue. The final frame piece included: a 1/4" hex bolt and nut that was drill-pressed and attached with cyanoacrylate glue and five layers of 1.5 cm thick maple wood layers stacked with glue. The Actuonix PQ12® linear actuator was securely attached using Command Strip® adhesives.

5.4 Neural Response Testing

The final ensemble of components - featuring worm specimen, crosslinked PEG gel, PFA tubing, linear actuator, and frame, shown in Figure 29 - was assembled over a fluorescence confocal microscope to validate its ability to measure a neural response to light stimulation. Once

baseline responses were verified, stretch stimuli were applied to the sample and subsequent responses were measured.

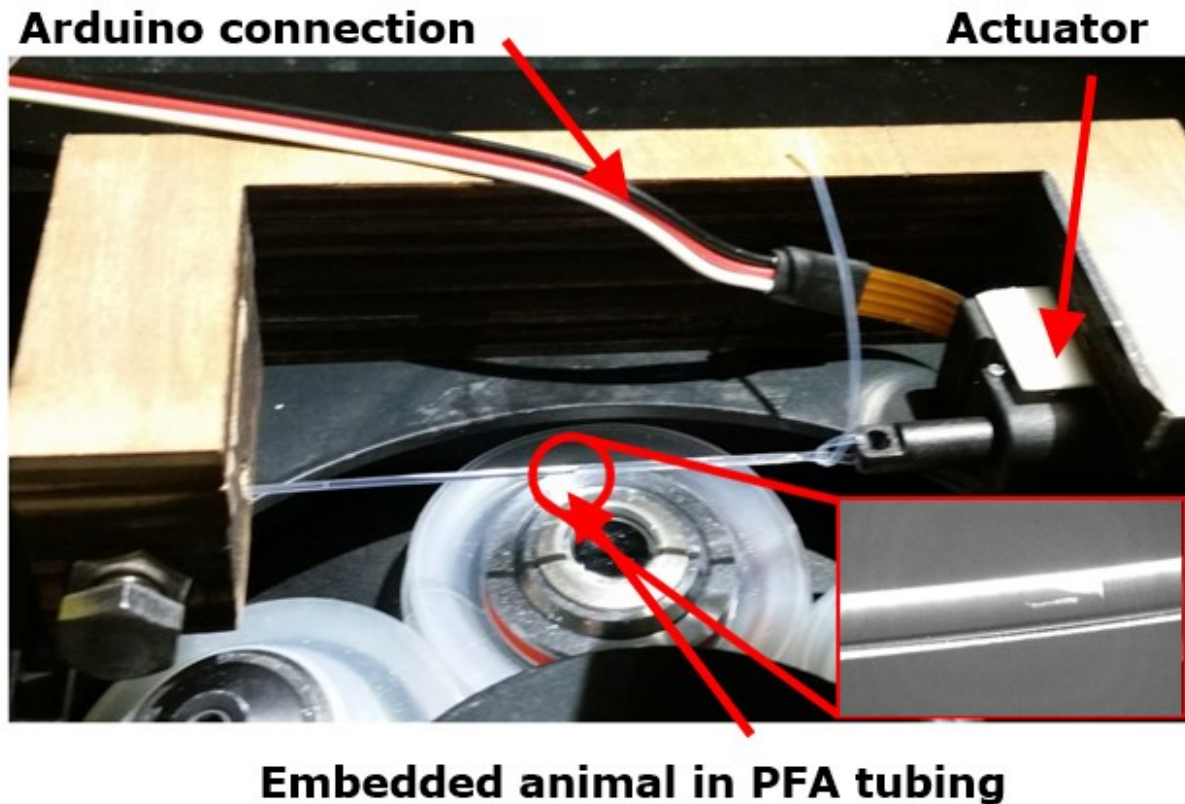


Figure 29: Full system ensemble

5.4.1 AWA Response Verification

A worm line with the olfactory AWA neuron genetically engineered to depolarize its calcium channels upon Chrimson light stimulation, as described by Larsch et al. (2015) [20], was made available for testing. These worms were seeded into the full ensemble shown in Figure 29, and stimulated with 605 nm red light in 5 second intervals once per minute for a 5 minute testing period. Corresponding changes in fluorescence, indicating increased calcium concentration (i.e. neural activity) triggered by the red light, were measured using MicroManager software.

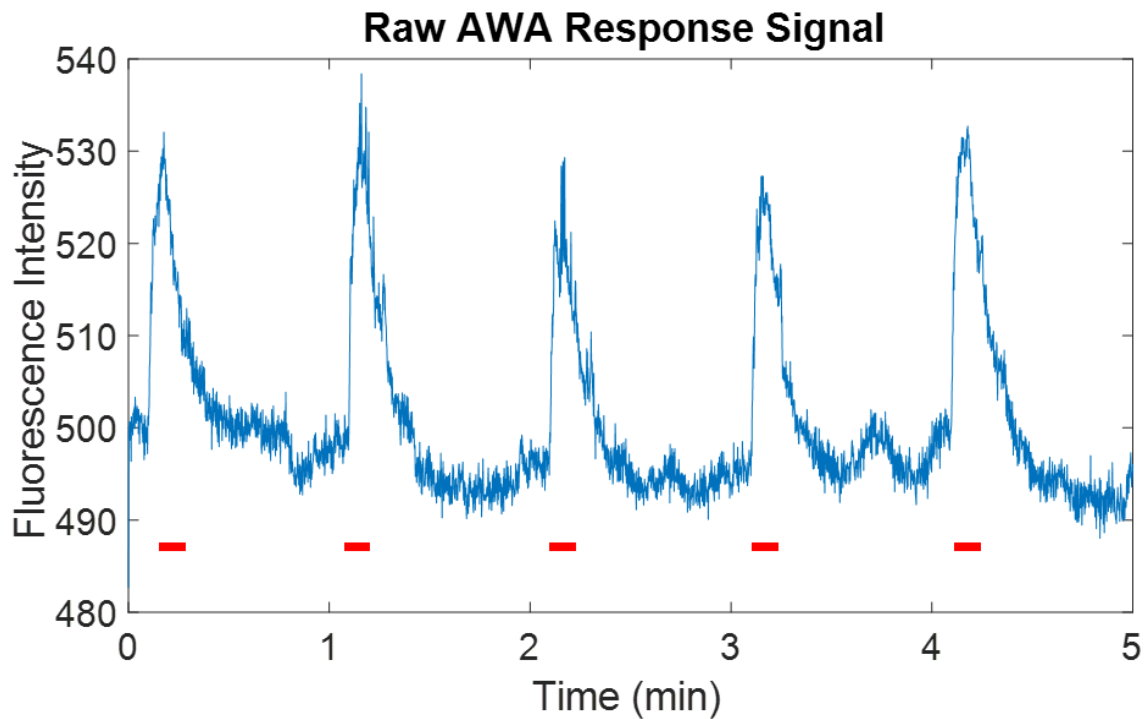


Figure 30: Raw AWA Response under Chrimson stimulation. Fluorescence peaks and descents correspond with each red light stimulation as indicated by the red bars

Figure 30 shows the raw AWA response to red light stimulation within the full ensemble. This produced defined peaks and decays in fluorescence as expected with the GCaMP-modified strain. Next, the design was verified by assessing whether a neural response like in the above image could also be achieved after delivering a stretch to the worm sample using the linear actuator. The tubing was stretched to 40% of actuator stroke arm length, corresponding to a 3.9% tube strain (Figure 23, tube stretch tests).

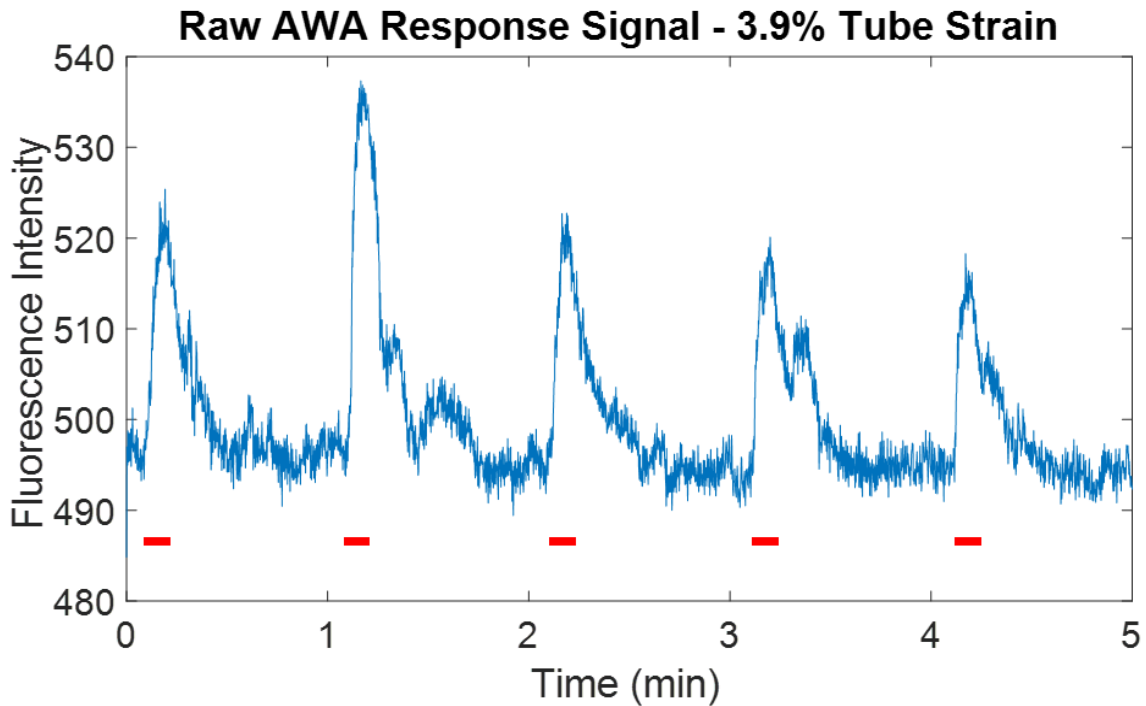


Figure 31: AWA Response under Chrimson stimulation post 3.9% stretch of tube

As in Figure 31 (first raw signal), the stretched AWA was also able to produce defined peaks in fluorescent activity corresponding to GCaMP activation via red light. Stretching the sample and refocusing on it did not limit its ability to be monitored optogenetically within the ensemble. Now that both no-stretch and stretch conditions were verified as capable of producing a neural response via Chrimson stimulation, experiments were designed analyzing changes in AWA activity with increasing tube strain. Moreover, the notable differences in peak height over the stimulation implies that activity and function were indeed affected by the tube strain.

5.4.2 AWA Response Experiments

Experiments were designed and conducted to monitor the AWA response with increasing tube strain delivered by the actuator. First, the tubing was stretched with 20% stroke arm increments. This prompted six experimental conditions - 0% pre-stretch, followed by five stretch iterations corresponding to 20%, 40%, 60%, 80%, and 100% stroke arm retraction. Using the data

collected from the tubing strain responses in Chapter 5.1, the stroke % was correlated to its corresponding tube strain. At each condition, targeted AWA neurons were stimulated with five 5-second Chrimson stimulation periods, and the subsequent quantitative neural response was measured as described before. Change in fluorescence was normalized to a baseline fluorescence value measured just prior to light stimulation.

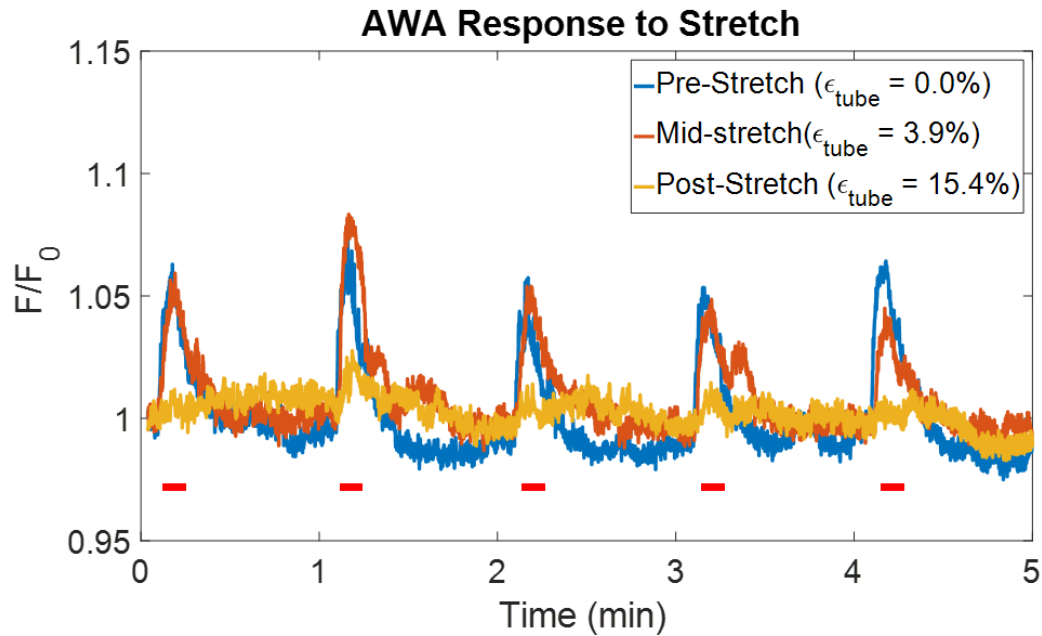


Figure 32: AWA Response with Stretch. Neural activity is measured as the change in fluorescence normalized to the initial baseline value

Figure 32 shows the AWA response of pre-stretch, mid-stretch and post-stretch conditions. The mid-stretch and post-stretch were matched to the corresponding tube strains of 3.9% and 15.4% respectively in order to correlate quantitative neural output with stretch. ImageJ measurement tools did not provide measurements of neuronal strain sufficient enough to reliably correlate neuronal strain directly to change in function.

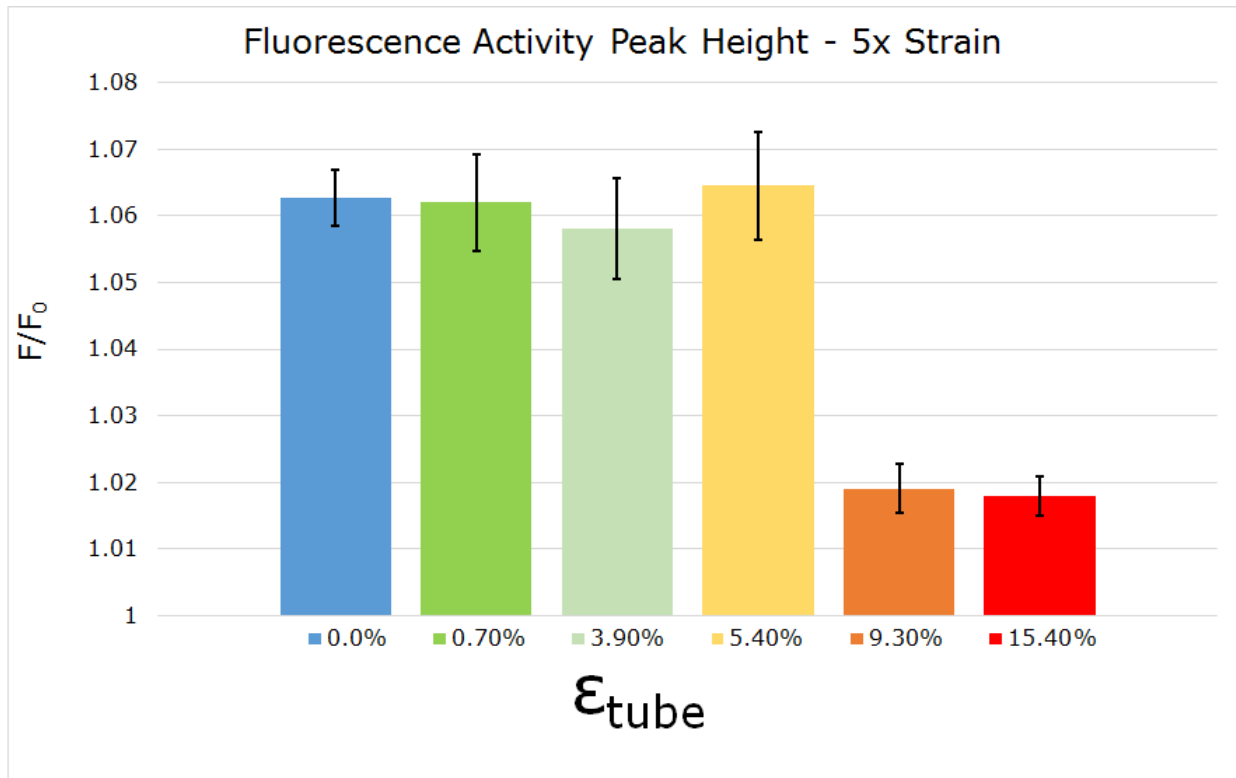


Figure 33: Average peak height of AWA normalized response with increasing tube strain

Comparing the six stretch conditions, normalized fluorescence peak height decreases sharply after exceeding 5.4% tube strain. Specifically, 5.4% tube strain produced peak height of 1.065 ± 0.008 comparable to peak heights at lower strains, however the 9.3% and 15.4% (post-stretch) conditions produced much smaller peaks of 1.019 ± 0.004 and 1.018 ± 0.003 respectively. This pattern of decrease in peak height appears to follow logarithmic decay - interestingly since tubing strained exponentially with stretch testing (Figure 23), this implies an inversely proportional relationship between tubing strain and AWA activity. Further analysis is provided in Chapter 7.

In addition to five stretch iterations, the full system was tested with two stretch iterations at 50% stroke (4.6% tube strain) and 100% stroke (15.4% tube strain).

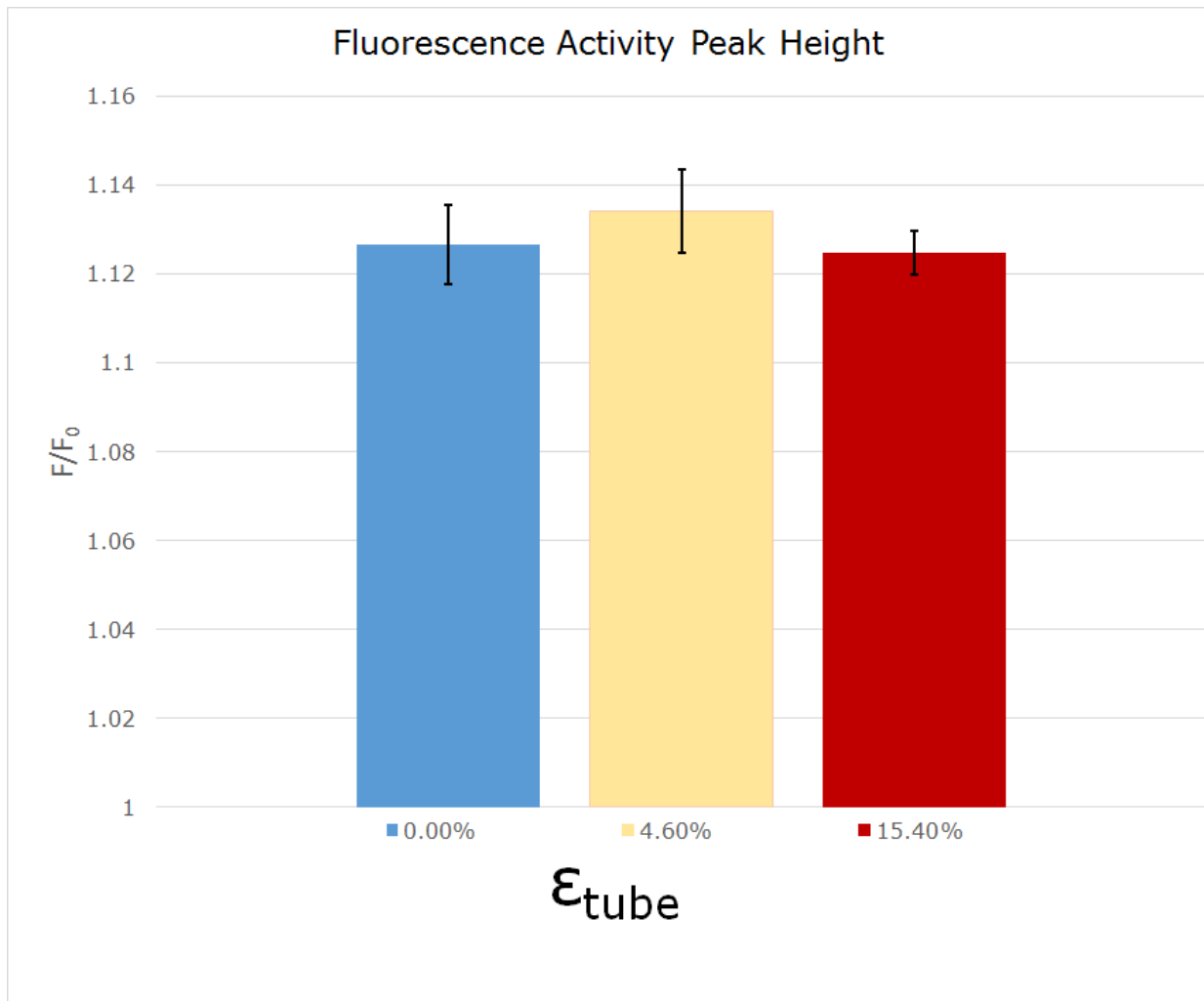


Figure 34: Average peak height of AWA normalized response with increasing tube strain

This trial of two stretch iterations shows much greater peak height than the trial with five stretch iterations. Neuronal activity did not decrease with increasing tubing stretch, as peak height did not alter significantly (Figure 35). Further discussion of the differences in neuronal response pattern between the two trials varying the number of stretch iteration follows in Chapter 7.

Chapter 6: Final Design and Validation

Our final design method, outlined in Ch. 5, was the tubing design involving polymeric tubing and linear actuation with a wooden frame will be validated in the sections below.

6.1 Final Protocol

The first step of the final design is to prepare the specimen for testing. This step includes pipetting a small amount of hydrogel onto a microscope plate so that *C. elegans* can be picked and transferred into the hydrogel. A small section of PFA tubing is cut and fed onto the nose of a syringe which allows for direct suction of the hydrogel solution into the tube. Ice can be applied to the outside of the tube to immobilize and elongate the animal(s). Once this is complete, the hydrogel can be UV crosslinked directly in the tube for about one minute.

In the next step, the tubing can be threaded through the actuator on one end, and fixed to the frame on the other end. The frame (with tubing and animal) can be set up on the microscope such that the specimen is within in the microscope field of view. The flashing blue light can be turned on and the Chrimson light setup can begin. This includes opening a MATLAB script and setting up the number and duration of pulses. The actuator should then be plugged into the Arduino board, with the appropriate code running on a separate laptop from the microscope computer. The Arduino code can be found in Appendix B.

At this point, the sample is ready for a stretch trial. This can be achieved by inputting actuator stroke length % using the serial monitor in Arduino. Actuator stroke retraction distances can be customized, but we mostly used 10% increments to ensure that the organism did not move out of the microscope field of view too quickly during stretching. MicroManager software was used to record a neural response after stretching. Once recording through MicroManager has begun, the MATLAB program should be run to initiate Chrimson light pulses. Recordings can be

saved as image stack files once data acquisition and light pulses are complete. To obtain the fluorescence graphs in our report, the ‘Intensity versus Time’ add-on in Micromanager’s ImageJ accessory was used. A more detailed protocol can be found in Appendix A.

This novel method of translating strain to a live organism’s neuron was developed with the goal of monitoring the neuronal response to strain in live time. This was successfully validated in tests recording the fluorescence of the AWA target neuron as reported in Chapter 5. The fluorescence emitted by the AWA neuron was observed to increase when the Chrimson light shone onto *C. elegans* samples embedded within the device.

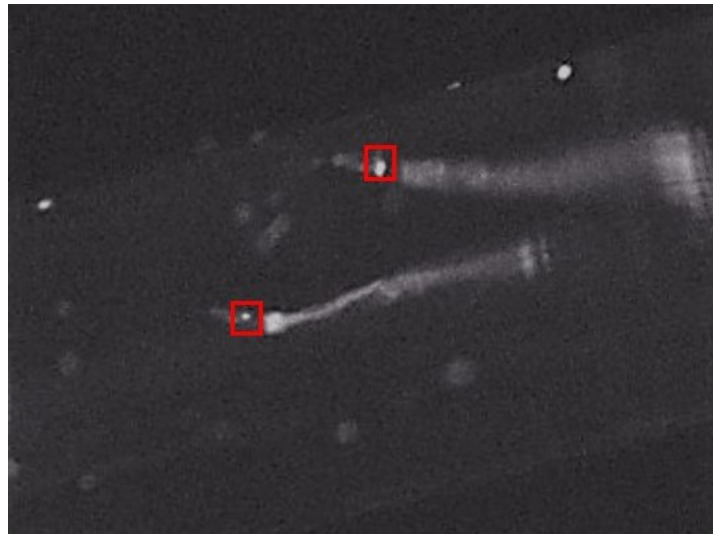


Figure 35: Fluorescence microscopy of Chrimson-activated AWA neuron (red boxes) in two *C. elegans*

In order for the device to meet the outlined objective, the organism must be aligned in a way that the neuron of interest can be imaged, which was met by aligning the organism in an optically transparent PFA tubing. Furthermore, to ensure the ability to image the organism over time, the organism must be fixed in place. This objective was met by immobilizing the organism when the PEG gel was crosslinked. The purpose of our device was to develop a correlation between strain and the activity of neurons. More specifically, we wanted to replicate the 10% strain experienced by neurons in a TBI incident. The actuator of our device was able to strain the tubing

at a maximum of 15%. Assuming the strain will translate directly from the tubing to the PEG gel and to the neuron, we have established an initial characterization of neural response to strain. A final objective was to quantify the neuronal function. This objective was met through the use of optogenetics, specifically modified GCaMP to increase calcium concentration upon red light stimulation. The neuronal function was quantified through the measurement of a change in fluorescence with respect to baseline, as shown by Figures 32 and 33.

6.2 *Design Standards*

Design standards pertaining to the experimentation performed in this project are outlined in Section 3.3. If the research tool we developed were to go into production, however, additional standards would need to be followed. ASTM F2900 – 11 would again have to be accounted for in commercial scale PEDGA formulations. Since polymeric tubing was a major component of our final design, standards concerning their tensile (ASTM D638, ISO527-2), compressive (ASTM D695, ISO604), and cyclic (ASTM D7774) loading capabilities would allow for translational analysis of mechanical stimuli to the embedded animal.

6.3 *Economics*

One of the most important outcomes of this project was the production of a transferrable frame piece, allowing for similar datasets to be produced on a variety of microscope setups in different laboratories. Our prototype worm-mounting setup was produced at a low cost. Initial investment was estimated at 80 USD, and cost per trial at 1.26 USD.

Table 12: Cost Analysis

Component	Price (USD)
Rapid prototyped frame (ABS filament)	\$10.00
Micro linear actuator	\$70.00
Each gel sample	\$1.00
5cm PFA tubing sample	\$0.13
Agar Plate	\$0.13
Initial investment	\$80.00
Cost per trial	\$1.26

Evidently, this research tool being available at an accessible cost to most laboratories helps potentiate its widespread use, with multiple laboratories operating the same setup to obtain strain response datasets corresponding to a variety of different experimental parameters. A large number of standardized data sets and high levels of collaboration can be achieved due to economic accessibility of this research tool, furthering the development of research towards characterization of mild to moderate traumatic brain injury.

6.4 Environmental Impact

The materials from which this research tool is produced were generally recyclable and biodegradable. The frame piece was manufactured from scrap wood. Additionally, PEG hydrogels are biodegradable, so the sample substrate (including embedded animals) can be disposed of in a low-impact fashion. The only higher impact consideration is the use of fluoropolymer based tubing to contain the substrate as non-biodegradable synthetic polymer. However, since PFA is a thermoplastic, it can be melted and reprocessed for long term recycling.

6.5 Societal Influence

Enhancing our understanding of TBI may serve to treat TBI in a more active way rather than the passive “rest-and-recover” method currently used for most injuries. Moreover, a deeper understanding of TBI developed through our product may steer society away from participating in activities that would result in TBI by raising awareness of the more long-term neurological impacts of repeated milder strains currently undefined and underdiagnosed in the clinic.

6.6 Political Ramifications

Since this product is a research tool, the political effect is minimal. New data made possible by this product could raise awareness of the struggles that professional athletes face today, specifically football players known to suffer from chronic traumatic encephalopathy (CTE). In a broad sense, the improvement of this research tool could lead to a better understanding of TBI, which affect the regulation of certain sports where TBI is most common, such as MMA, football, and soccer.

6.7 Ethical Concerns

The final deliverable of this project provides an avenue for TBI datasets to be generated without compromising the health of human subjects. *In vivo* experimentation for TBI usually encompasses the use of mice and rats to determine the bulk mechanical forces and acceleration required to induce severe injury. However, studying the long term biological effects of moderate injury within large *in vivo* systems such as rats can be difficult because electrodes would be required to quantify potential degradation in cellular activity. Alternatively, optogenetics could be employed, but it would have to be in an invasive manner since imaging through fur and skin cannot be done with a simple microscope. Invasive neural response monitoring over the long term would result in discomfort to mammalian systems being studied.

Use of *C. elegans* as a model organism addresses ethical concerns by allowing for continuous monitoring of neural, cellular level activity through a transparent organism, without causing discomfort and unethical experimentation to occur with mammalian systems - including humans. Over time, the goal is to develop this system into one comprehensive enough to replace live mammals as physical models for traumatic brain injury.

6.8 Health & Safety Issues

C. elegans cultures are non-pathogenic, assuming contamination of agar plates is managed appropriately. Sterilization protocol was followed at all times for the worm picking tool, and old plates were disposed of safely in hazardous waste bins. Precautionary measures aside, the process for data sampling is inherently low risk to operators and bystanders. Loading the samples involves the use of a simple luer lock syringe. Precautionary measures were taken during photocrosslinking to shield the eyes from the damaging effects of high frequency radiation. The device and sample were covered with aluminum foil, and safety goggles were used. Beyond crosslinking steps, low risk was involved with operating the microscope and the small moving parts of the micro linear actuator.

6.9 Manufacturability

There is no applicable way to manufacture this product on a large scale. It is possible to produce a tube stretching device that can be manufactured specific to each customer but on a much smaller scale than mass manufacturability. The product would need to be modified to tailor to individual specifications based on the researcher's purposes. The product would target cell or nematode organism stretching devices, as well as adapting to incorporate microfluidic channels.

6.10 Sustainability

This research tool is manufactured from inexpensive materials and will remain effective for a long period of time after the initial investments. As discussed in the economics section, the up-front cost of the unit is \$80. Considering the unit is transferable between different microscopes, a given laboratory would only need to own one unit for it to be able to obtain sufficient data sets. Researchers would need to invest in tubing periodically and would need to procure the appropriate worm lines to use for experimentation, depending on which neurons they would like to test. Beyond the tubing and animals, the rest of the apparatus is permanent. Moreover, the sustainability of consistent manufacturing for this simple device will allow for controlled testing parameters. This will allow for different labs to collaborate on similar experiments, allowing for consistent data sets to be obtained towards neurochemical research pertaining to traumatic brain injury.

Chapter 7: Discussion

7.1 Neural Signal Degeneration

While previous work has studied TBI models and provided information on the cellular scale to injury, the developed device allows for the study of how single cells respond to strain in a novel way. The initial result obtained with our platform indicates a decrease in AWA activity with increasing tubing strain. Neural activity peak magnitude remained mostly constant for controls, but after straining the tubing about 4%, peak magnitude increased on the first two red light pulses, followed by decreasing magnitudes in the remaining three pulses. This suggests an increase in neural stimulation shortly after the stretch stimuli, but a lower average peak magnitude compared to control suggests decrease in neuronal activity as calcium concentrations just outside the neurons diminishes. Neural activity decreased to a greater extent when tubing is strained to 15.4% - Here, the change in fluorescence to baseline ratio is 1.01 as the stretch stimuli have exhausted the neuron's ability to depolarize. The near "flat-lining" of neural activity implies that there may exist a strain threshold between 3.9% and 15.4% of tubing strain that will lead to debilitation of AWA neuron. Assuming direct translation of strain from tubing to the neuron and decrease in calcium concentration to be indicative of neuronal function, this result begins to characterize neuronal response to strain. Given that Chrimson and GCaMP were both present in the same cell, the tube strain appeared to act as an inhibitory mechanism for calcium signaling since GCaMP's calcium-to-fluorescence conversion dropped so dramatically post-stretch while depolarization by Chrimson remained constant for all conditions. Additional studies examining the effect of strain on GCaMP and Chrimson stimulation in multiple neurons could provide insights into neuronal communication by for example, conducting experiments with Chrimson stimulation of AWA and GCaMP measurement in AIB, an interneuron known to form synapses with AWA in a sensory circuit.

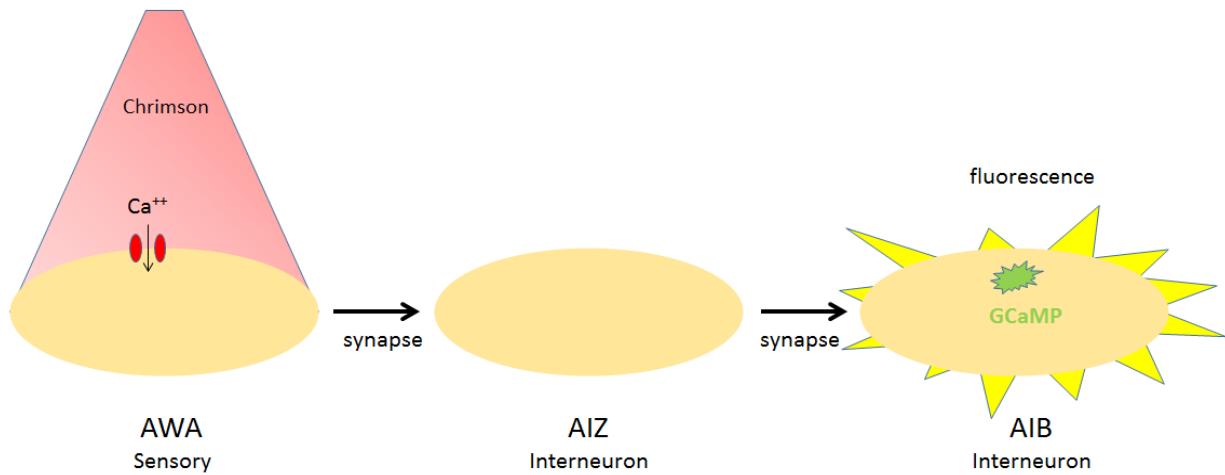


Figure 36: Hypothetical Neural Response Schematic for AWA Circuit

7.2 Data Limitations

However, in order to reliably establish the implied threshold, there are several limitations to the current design that must be addressed to more accurately and easily characterize these functional strain responses. First, the PFA tubing used deforms plastically on the first stretch cycle. Fully characterizing the neural response to strain will require cyclic testing, which will be made possible by more elastic tubing that nonetheless satisfies the size and crosslinking requirements established in Chapter 4. Secondly, the determination of this neuronal strain-function relationship from our data depends on the presumption that tube strain directly translates to neuron strain, but this could not be confirmed reliably using images. Future work can utilize imaging algorithms, as well as 3D imaging techniques, to measure the relative size of a fluorescently labeled neuron and measure how its size changes (i.e. how the neuron strains). Obtaining quantitative measures of neuron strain permits the discovery of more clinically relevant data, as the neuronal strain of a model organism with neurochemical homology to mammalian brains, like *C. elegans*, can be directly correlated to neuronal strains seen in both real life impacts and those simulated in

computational models. The designed platform did not always provide clear image resolution (Figure 38). This was due to the worm and tube orientation in the vertical Z-plane.

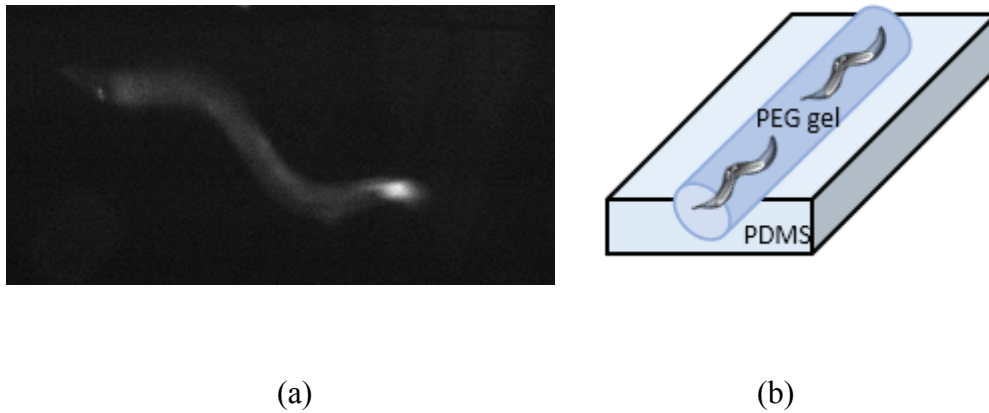


Figure 37: (a) Example of fluorescent image with poor resolution and (b) a potential solution using a microfluidic channel in PDMS master in which to seed crosslinked gel and animals

This issue was addressed by re-drilling holes in the frame to better align the tubing, but still produced images that lacked resolution sufficient for measuring neural activity at 10x magnification. In the future, this issue could be solved by the use of a microfluidic channel in a PDMS master that provides a flat, transparent surface through which to image in a level Z-plane and the channel in which to seed crosslinked PEG gel and animals. Furthermore, using our setup on a 3-D imaging platform such as diSPIM could greatly ameliorate neuronal resolution in the Z-plane. This improvement would particularly prove advantageous for monitoring responses in the DVA proprioceptor, whose image quality in our current setup was assessed (Figure X). One future improvement is to improve the quality of neuronal imaging through the use of dual-view inverted selective plane illumination microscopy (diSPIM). This form of microscopy uses a light sheet to illuminate a plane for live time viewing. This allows for complex organisms to be viewed in volumetric 4D with subcellular resolution [53]. Furthermore, diSPIM has the advantage of preserving the specimen under investigation in comparison to confocal microscopy. The diSPIM

illuminates a planar cross section of the specimen as opposed to the entire specimen thus protecting it from photo bleaching. With diSPIM a water-dipped objective is used that is perpendicular to the light emitting objective. A piezoelectric stage keeps the sample in focus as it is scanned with the fluorescent light sheet [53]. The limitations of the diSPIM include the precise adjustments and fine tuning required to view a specimen. LSM has the most success with small (50 - 60 micron), transparent specimens such as *C. elegans* embryos or single cell layers [44]. Imaging of microscopic neuronal samples could also be obtainable through light sheet laser scanning microscopy (LSM) with improved resolution. However, LSM is limited by its penetration depth in heterogeneous samples such as in live organisms. LSM also has a large difference between lateral and axial resolutions [44].

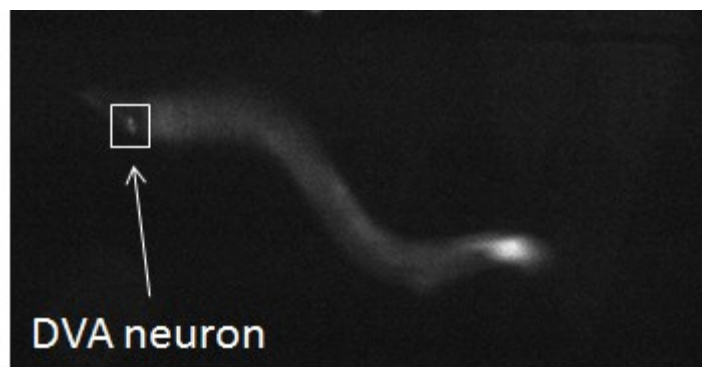


Figure 38: Poor image resolution of the DVA neuron

However, loss of image focus during stretch coupled with insufficient neuronal resolution confounded this test. DVA, as a proprioceptor running the length of the worm body, would serve as an excellent experimental control for characterizing neuronal response to stretch, so revising the design to permit DVA response measurement under a 3-D imaging platform *while stretching* would greatly expand the possibilities for experiments that would build on our initial findings. Achieving this goal is facilitated by the frame's transferability to different microscope stages, including potentially a 3-D platform such as diSPIM.

7.3 Achievement of Objectives

7.3.1 Successful aspects of design

Despite these limitations and opportunities for future improvement, it is important to highlight how project objectives were met. The principal objectives to house an animal, stretch, and record neuronal activity output quantitatively were achieved. More specifically, worms were immobilized into an optically transparent medium that permitted measuring the changes in neural activity, as indicated by fluorescence, with a confocal fluorescence scope. In addition, the actuator allowed the controlled delivery of strain magnitudes, beyond the goal of 10%, as they relate to the stroke arm length which were correlated to the tubing strain. This supplied an initial connection between tubing strain and a measurable functional response in the AWA neuron using our system. Furthermore, this entire setup was made possible by the frame piece, which satisfies an additional objective by allowing transferal between scopes, potentially including a diSPIM platform, by combining all components (tubing and actuator) into one piece. While the desired datasets cannot be obtained with the current design, it successfully meets the principal objectives established, as well as multiple sub-objectives and “want-to-have features” established in Chapter 3.

7.3.2 Novelty

The unique aspect of this project is that it is the first which involves the analysis of worm neural response to tensile strains. The only other projects which have analyzed the neural response to strains have been in compression, or have only examined the bulk mechanical properties of *C. elegans*. This project, therefore, fills a new niche for the type of mechanobiological studies which can be performed using *C. elegans* as a model neurochemical homologue to the mammalian brain. Now, tensile studies can be performed in conjunction with compressive studies to create complete

datasets simulating tissue strain due to injury, in accordance with the combination of both strain types in real TBI situations.

7.3.3 Assumptions

Throughout our experimental process, certain assumptions were made in order to continue development and data acquisition. The first major assumption we had to make was that strain applied to the tubing would (1) apply directly to the embedded hydrogel segment within, and (2) gel strain would apply directly to the worm and its relevant uniaxial neurons. We were able to verify that gel stretch will result in worm stretch through initial trials involving the PDMS slab with a gel disc on top.

7.3.4 Iteration through objectives

We managed to achieve the first main objective of the project, immobilizing the worm in an optically transparent medium, by designing and improving a protocol for embedding a worm in a PEG hydrogel. We used this medium under fluorescence microscopy to verify that neural responses can indeed be viewed and recorded through our substrate of choice. This was achieved through the imaging of whole brain imaging worms under rhodamine stimulation, and through GCaMP signal monitoring. We calculated the force parameters required of our linear actuator, and once obtained, we tested the strain it can produce on our substrate materials. Finally, all of the listed components were synchronized in testing trials, allowing us to observe a change in the neuronal function of a non-proprioceptive neuron post stretch.

Chapter 8: Conclusions & Recommendations

We have developed an initial platform to seed immobilized animals, mechanically actuate and quantitatively record neural output. Using this platform, we collected an initial dataset suggesting a decrease in neuronal function with increasing strain. Upon repeated testing and improvements to the current design, additional experiments will build on the initial result with the goal of reliably and accurately characterizing the neuronal response to strain.

Another potential future improvement is the use of elastic tubing material that still permits crosslinking will allow for cyclic testing, an important testing method for understanding this relationship between strain and function. Cyclic loading can simulate repeated concussions, which has been shown to be the leading cause of chronic traumatic encephalopathy (CTE) in professional football athletes and war veterans [46]. Improving the actuation capabilities to deliver more controllable strain magnitude and rate will also enhance the ability of our design to serve as a platform to perform experiments modifying various strain magnitudes, rates, durations, and cycles. Lastly, methods to level the Z-plane orientation of the neuronal sample will allow for more consistent and efficient workflow and results. Methods for orientation of worms in the Z-axis can include guiding the worm into position through the use of microfluidic channels. Neuron-tracking software can ensure neural response monitoring while stretching, an important facet to understanding neuronal communication.

Incorporating all of these improvements will create a testing platform optimal to designing diverse mechanobiological experiments and collecting results. This testing will answer valuable questions that could lead to discovery of neuronal responses clinically relevant to CTE and TBI patients - for example, what is the temporal effects of repeated neural strains? Are injuries permanent or temporary? At what injury threshold? How does response differ between “traumatic”

and “milder” strains? How do they affect neuronal communication and circuitry? Many of these questions can be addressed with improvements to testing. One such improvement to polymeric tubing elasticity would allow not only for cyclic tests to simulate neuronal tissue moving back and forth, but for the sample to be fully relaxed after testing, which would help determine whether or not injuries are permanent.

Our initial result indicates how neuronal activity of a single AWA neuron may be altered upon strain, but what knowledge can be gained by looking at other neurons, or multiple neurons simultaneously? A potential starting point for answering these questions centers on DVA, the long proprioceptor neuron that would act as an experimental control. With DVA’s circuits fully documented, experiments monitoring responses in interneurons in a DVA circuit during strain will characterize the strain’s effect of neuronal communication. Since modern imaging of encephalopathic patients has revealed global effects of strain on many regions of neural tissue, studying the effects on neuronal communication will reveal how neural circuits connecting to distinct brain regions may degenerate as a result of injury.

In a broad sense, this project addresses the need to enhance understanding of neural functional response to strains characteristic of traumatic impact. Current computational models can effectively calculate how neural tissues will strain with a simulated impact. Future work is necessary to understand how neural function is affected by repeated straining at the biological level such as common in contact sports. Our testing platform serves as an initial step in providing a research tool to characterize this, and eventually to improving the clinical relevance and predictive efficacy of TBI computational models. Improved models will ultimately lead to an increased understanding of the biological effects of injury, leading to the development of new preventative equipment and protocol, as well as medications to treat chronic conditions.

References

- [1] M. Faul *et al.* Traumatic brain injury in the United States: National estimates of prevalence and incidence, 2002-2006. *Injury Prevention* 16(Supplement 1), pp. A268. 2010. Available: <http://search.proquest.com/docview/1780958125>. DOI: 10.1136/ip.2010.029215.951.
- [2] D. F. Meaney, B. Morrison and C. Dale Bass. The mechanics of traumatic brain injury: A review of what we know and what we need to know for reducing its societal burden. *Journal of Biomechanical Engineering* 136(2), pp. 21008. 2014. Available: <http://www.ncbi.nlm.nih.gov/pubmed/24384610>. DOI: 10.1115/1.4026364.
- [3] K. L. Johnson *et al.* Constrained topological optimization of a football helmet facemask based on brain response. *Materials & Design* 111pp. 108-118. 2016. . DOI: 10.1016/j.matdes.2016.08.064.
- [4] S. Ji *et al.*, "Parametric comparisons of intracranial mechanical responses from three validated finite element models of the human head," *Ann. Biomed. Eng.*, vol. 42, pp. 11-24, January 01, 2014.
- [5] A. C. Bain and D. F. Meaney, "Tissue-level thresholds for axonal damage in an experimental model of central nervous system white matter injury," *J. Biomech. Eng.*, vol. 122, pp. 615-622, December 01, 2000.
- [6] A. C. Bain, R. Raghupathi and D. F. Meaney, "Dynamic stretch correlates to both morphological abnormalities and electrophysiological impairment in a model of traumatic axonal injury," *J. Neurotrauma*, vol. 18, pp. 499-511, May 01, 2001.
- [7] E. Bar-Kochba *et al.*, "Strain and rate-dependent neuronal injury in a 3D in vitro compression model of traumatic brain injury," *Sci. Rep.*, vol. 6, pp. 30550, August 02, 2016.
- [8] S. J. Park, M. B. Goodman and B. L. Pruitt, "Analysis of nematode mechanics by piezoresistive displacement clamp," *Proc. Natl. Acad. Sci. U. S. A.*, vol. 104, pp. 17376-17381, October 30, 2007.
- [9] M. Malkoch *et al.*, "Synthesis of well-defined hydrogel networks using click chemistry," *Chem. Commun. (Camb)*, vol. (26), pp. 2774-2776, July 14, 2006.
- [10] J. T. Weber, "Altered calcium signaling following traumatic brain injury," *Front. Pharmacol.*, vol. 3, pp. 60, April 12, 2012.
- [11] (Sep 22,). *Traumatic brain injury (TBI) - definition and pathophysiology: Overview, Epidemiology, primary injury*. Available: <http://emedicine.medscape.com/article/326510-overview>.
- [12] F. Hernandez, P. B. Shull and D. B. Camarillo. Evaluation of a laboratory model of human head impact biomechanics. *Journal of Biomechanics* 48(12), pp. 3469-3477. 2015. Available: <http://www.sciencedirect.com/science/article/pii/S0021929015003243>. DOI: 10.1016/j.jbiomech.2015.05.034.
- [13] M. de Bono and A. V. Maricq, "Neuronal substrates of complex behaviors in *C. elegans*," *Annu. Rev. Neurosci.*, vol. 28, pp. 451-501, 2005.
- [14] T. Kaletta and M. O. Hengartner, "Finding function in novel targets: *C. elegans* as a model organism," *Nat. Rev. Drug Discov.*, vol. 5, pp. 387-398, May 01, 2006.
- [15] R. A. Kerr. Imaging the activity of neurons and muscles. *WormBook : The Online Review of C. elegans Biology* pp. 1. 2006. Available: <http://www.ncbi.nlm.nih.gov/pubmed/18050440>. DOI: 10.1895/wormbook.1.113.1.
- [16] *Nervous System General Description*. Available: <http://www.wormatlas.org/hermaphrodite/nervous/Neuroframeset.html>.
- [17] R. M. Durbin, *Studies on the Development and Organisation of the Nervous System of Caenorhabditis Elegans*, 1987.
- [18] Anonymous "Syntaxin: A Synaptic Protein Implicated in Docking of Synap," *Science*, vol. 257, pp. 255, .
- [19] (Nov 26,). *DVA*. Available: <http://www.wormatlas.org/neurons/Individual%20Neurons/DVAframeset.html>.
- [20] J. Larsch *et al.*, "A Circuit for Gradient Climbing in *C. elegans* Chemotaxis," *Cell. Rep.*, vol. 12,

- pp. 1748-1760, September 22, 2015.
- [21] M. Mank *et al.*, "A FRET-based calcium biosensor with fast signal kinetics and high fluorescence change," *Biophys. J.*, vol. 90, pp. 1790-1796, March 01, 2006.
- [22] M. G. Erickson *et al.*, "FRET two-hybrid mapping reveals function and location of L-type Ca²⁺ channel CaM preassociation," *Neuron*, vol. 39, pp. 97-107, July 03, 2003.
- [23] H. Suzuki *et al.*, "In vivo imaging of *C. elegans* mechanosensory neurons demonstrates a specific role for the MEC-4 channel in the process of gentle touch sensation," *Neuron*, vol. 39, pp. 1005-1017, September 11, 2003.
- [24] C. Grienberger and A. Konnerth, "Imaging calcium in neurons," *Neuron*, vol. 73, pp. 862-885, March 08, 2012.
- [25] A. H. Kahn-Kirby and C. I. Bargmann. TRP channels in *C. elegans*. *Annual Review of Physiology* 68pp. 719. 2006. Available: <http://www.ncbi.nlm.nih.gov/pubmed/16460289>.
- [26] W. Gilpin, S. Uppaluri and C. P. Brangwynne, "Worms under Pressure: Bulk Mechanical Properties of *C. elegans* Are Independent of the Cuticle," *Biophys. J.*, vol. 108, pp. 1887-1898, April 21, 2015.
- [27] N. B. Angstman *et al.* High interindividual variability in dose-dependent reduction in speed of movement after exposing *C. elegans* to shock waves. *Frontiers in Behavioral Neuroscience* 9pp. 12. 2015. Available: <http://www.ncbi.nlm.nih.gov/pubmed/25705183>. DOI: 10.3389/fnbeh.2015.00012.
- [28] PDMS: A Review. Available: <http://www.elflow.com/microfluidic-tutorials/microfluidic-reviews-and-tutorials/the-poly-di-methyl-siloxane-pdms-and-microfluidics/>.
- [29] D. A. Markov *et al.*, "Variation in diffusion of gases through PDMS due to plasma surface treatment and storage conditions," *Biomed. Microdevices*, vol. 16, pp. 91-96, February 01, 2014.
- [30] F. Ullah *et al.*, "Classification, processing and application of hydrogels: A review," *Mater. Sci. Eng. C. Mater. Biol. Appl.*, vol. 57, pp. 414-433, December 01, 2015.
- [31] Y. Okumura and K. Ito. The polyrotaxane gel: A topological gel by figure-of-eight cross-links. *Advanced Materials* 13(7), pp. 485-487. 2001. . DOI: AID-ADMA485>3.0.CO;2-T.
- [32] K. Haraguchi and T. Takehisa. Nanocomposite hydrogels: A unique Organic-Inorganic network structure with extraordinary mechanical, optical, and swelling/de-swelling properties. *Advanced Materials* 14(16), pp. 1120. 2002. . DOI: AID-ADMA1120>3.0.CO;2-9.
- [33] T. Nonoyama and J. P. Gong, "Double-network hydrogel and its potential biomedical application: A review," *Proc. Inst. Mech. Eng. H.*, vol. 229, pp. 853-863, December 01, 2015.
- [34] E. M. Ahmed, "Hydrogel: Preparation, characterization, and applications: A review," *J. Adv. Res.*, vol. 6, pp. 105-121, March 01, 2015.
- [35] Jeong-Yun Sun *et al.* Highly stretchable and tough hydrogels. *Nature* 489(7414), pp. 133. 2012. Available: <http://www.ncbi.nlm.nih.gov/pubmed/22955625>.
- [36] S. J. Buwalda *et al.* Hydrogels in a historical perspective : From simple networks to smart materials. *Journal of Controlled Release* 190pp. 254. 2014. Available: <http://www.narcis.nl/publication/RecordID/oai:dspace.library.uu.nl:1874%2F303491>.
- [37] A. K. O'Brien, N. B. Cramer and C. N. Bowman. Oxygen inhibition in thiol-acrylate photopolymerizations. *Journal of Polymer Science Part A: Polymer Chemistry* 44(6), pp. 2007-2014. 2006. . DOI: 10.1002/pola.21304.
- [38] J. Zheng *et al.*, "Strain-Promoted Crosslinking of PEG-based Hydrogels via Copper-Free Cycloaddition," *ACS Macro Lett.*, vol. 1, pp. 1071-1073, August 21, 2012.
- [39] F. W. Giacobbe, "Oxygen permeability of teflon-PFA tubing," *J Appl Polym Sci*, vol. 39, pp. 1121-1132, 1990.
- [40] (Apr 16.). *What's the difference between pneumatic, hydraulic, and electrical actuators?*. Available: <http://machinedesign.com/linear-motion/what-s-difference-between-pneumatic-hydraulic-and-electrical-actuators>.
- [41] Y. Shao *et al.* Uniaxial cell stretching device for live-cell imaging of mechanosensitive cellular functions. *The Review of Scientific Instruments* 84(11), pp. 114304. 2013. Available: <http://www.ncbi.nlm.nih.gov/pubmed/24289415>. DOI: 10.1063/1.4832977.
- [42] J. P. Nguyen *et al.*, "Whole-brain calcium imaging with cellular resolution in freely behaving *Caenorhabditis elegans*," *Proc. Natl. Acad. Sci. U. S. A.*, vol. 113, pp. 1074, February 23,

- 2016.
- [43] S. Sterman and J. G. Marsden, "SILANE COUPLING AGENTS," *Ind. Eng. Chem.*, vol. 58, pp. 33-37, 1966.
- [44] R. Prevedel *et al*, "Simultaneous whole-animal 3D imaging of neuronal activity using light-field microscopy," *Nat. Methods*, vol. 11, pp. 727-730, July 01, 2014.
- [45] A. Solladié-Cavallo and J. Suffert. Synthesis of optically pure perfluoroalkyl aryl carbinols. *Synthesis* 1985(6/7), pp. 659-662. 1985. Available: <http://www.thieme-connect.de/DOI/DOI?10.1055/s-1985-31298>. DOI: 10.1055/s-1985-31298.
- [46] B. Omalu *et al*, "Chronic traumatic encephalopathy in an Iraqi war veteran with posttraumatic stress disorder who committed suicide," *Neurosurg. Focus.*, vol. 31, pp. E3, November 01, 2011.
- [47] McKenzie, Catherine K., Inmaculada Sanchez-Romero, and Harald Janovjak. "Flipping The Photoswitch: Ion Channels Under Light Control". *Advances in Experimental Medicine and Biology* (2015): 101-117. Web. 26 Apr. 2017.
- [48] J. Larsch *et al*, "High-throughput imaging of neuronal activity in *Caenorhabditis elegans*," *Proc. Natl. Acad. Sci. U. S. A.*, vol. 110, pp. 4266, November 05, 2013.
- [49] L. Tian *et al*, "Imaging neural activity in worms, flies and mice with improved GCaMP calcium indicators," *Nat. Methods*, vol. 6, pp. 875-881, December 01, 2009.
- [50] *Federal Motor Vehicle Safety Standards and Regulations*. (2017). *Nhtsa.gov*. Retrieved 25 April 2017, from <http://www.nhtsa.gov/cars/rules/import/FMVSS/index.html>
- [51] Torgersen, J., Qin, X. H., Li, Z., Ovsianikov, A., Liska, R., & Stampfl, J. (2013). Hydrogels for Two-Photon Polymerization: A Toolbox for Mimicking the Extracellular Matrix. *Advanced Functional Materials*, 23(36), 4542-4554.
- [52] Heggers, J. P., Kossovsky, N., Parsons, R. W., Robson, M. C., Pelley, R. P., & Raine, T. J. (1983). Biocompatibility of silicone implants. *Annals of plastic surgery*, 11(1), 38-45.
- [53] Verveer, P. J., Swoger, J., Pampaloni, F., Greger, K., Marcello, M., & Stelzer, E. H. (2007). High-resolution three-dimensional imaging of large specimens with light sheet-based microscopy. *Nature methods*, 4(4), 311-313.

Appendix A: Neural Response Testing Protocol

This protocol provides step-by-step instructions for conducting *C. elegans* neural response testing using our setup.

Preparation:

1. Pipette 5 μ L of 20wt% PEGDA hydrogel solution onto hydrophobically treated surface.
2. Sterilize platinum pick with flame.
3. Pick 3-5 animals and transfer to PEGDA droplet.
4. Cut a 10 cm section of AWG no.24 FEP tubing.
5. Slide one end of tubing onto syringe needle.
6. Carefully suction the hydrogel droplet with transferred animals up to about halfway along the tubing section length.
7. Immobilize animals by gently placing tubing section on ice for 1 minute (making sure to isolate the animal to the center of the PEG liquid.)
8. Crosslink PEGDA by exposing tubing section to 350 nm UV light for 1 minute.
9. Verify crosslinking by applying pressure to syringe plunger. If the gel segment does not move, it has crosslinked properly.
10. Slide tubing off of syringe needle.
11. Carefully thread the tubing through the marked hole on the stage frame.
12. Tie the other end of the tubing to the end of the actuator arm. Do this such that the gel segment stays between either leg of the frame.
13. Pull the section hanging through the marked hole taught to ensure it is parallel to the stage but do not introduce and tension.
14. Secure the tubing in its proper alignment with the bolt that runs perpendicular to the marked hole.

Imaging:

1. Place frame with secured tubing containing crosslinked gel and animals onto microscope stage.
2. Turn on microscope and accompanying imaging tools and softwares.
3. Identify candidate worm for neural response testing and focus scope on it at 10x magnification.
4. Set to flashing blue light (exposure, etc.)

Programming red light pulse

1. In Matlab, change the ‘ ’ command in the ‘GeneratePulse.m’ file to tailor your pulse width, pulse interval, etc.)
2. Aim the red light over the sample on the scope stage.
3. Click ‘Run’ to run the script, generating the red light at the prescribed settings.

Operating the actuator

1. Plug in Actuonix PQ12 actuator to Arduino Uno board, and the board to the computer.
2. Using Arduino IDE, upload ‘sketch_feb221.ino’ code.
3. Verify that the board is set to the correct COM port and open the Serial Monitor.
4. Deliver strain as percent of the __ m stroke arm, by typing the percent as a positive integer (i.e. strain 10% = 0.1 = ‘10’) into the Serial Monitor.

Recording neural response:

1. Once ready to record neural response, click ‘Multi-D Aq’ in MicroManager.
2. Modify the sample number and sample rate to meet data acquisition needs. Identify
3. Click ‘Acquire!’ to begin recording (run Step 20 simultaneously to begin red light stimulation shortly after image acquisition begins).
4. The worm’s z-axis orientation may change after each stretch iteration, putting it out of focus. Take this account when programming pulse and stretch intervals so that enough time is given between red light pulses and stretches to refocus the objective on the worm.
5. After acquisition is complete, save your image files as an image stack.
6. Display fluorescence data by clicking ‘Plugins’ > ‘Intensity versus Time’. Save your fluorescence data as a .txt file for data analysis.

Appendix B: Arduino Code for Micro Linear Actuator

```

#include <Servo.h>

Servo myServo;
#define PIN_SERVO (9)
void SetStrokePerc(float strokePercentage)
{
  if ( strokePercentage >= 0.01 && strokePercentage <= 99.99 )
  {
    int usec = 1000 + (strokePercentage/100.0) * ( 1000 );
    myServo.writeMicroseconds( usec );
  }
}
void SetStrokeMM(int strokeReq,int strokeMax)
{
  SetStrokePerc( ((float)strokeReq) / strokeMax );
}
void setup()
{
  myServo.attach(PIN_SERVO);
  Serial.begin(9600);
}

void loop()
{
  // if there's any serial available, read it:
  while (Serial.available() > 0) {

    int strain = Serial.parseInt();

    Serial.print("Current stroke: ");
    Serial.print(strain);
    Serial.println("%");
    Serial.print("Current stroke length: ");
    Serial.print((strain / 100) * 28);
    Serial.println("mm");
    Serial.println();

    int usec = 1000 + (strain/100.0) * ( 1000 );
    myServo.writeMicroseconds( usec );
  }

}

#include <Servo.h>
Servo myServo;
#define PIN_SERVO (9)

void SetStrokePerc(float strokePercentage)
{
  if ( strokePercentage >= 1.0 && strokePercentage <= 99.0 )
  {
    int usec = 1000 + (strokePercentage/100.0) * ( 1000 );
    myServo.writeMicroseconds( usec );
  }
}

```

```
void SetStrokeMM(int strokeReq,int strokeMax)
{
  SetStrokePerc( ((float)strokeReq) / strokeMax );
}

void setup()
{
  myServo.attach(PIN_SERVO);
  Serial.begin(9600);
}

void loop()
{
  // if there's any serial available, read it:
  while (Serial.available() > 0) {

    int strain = Serial.parseInt();
    int slength = (strain/100)*28;
    Serial.print("Current stroke: ");
    Serial.print(strain);
    Serial.println("%");
    Serial.print("Current stroke length: ");
    Serial.print(slength);
    Serial.println("mm");
    Serial.println();

    int usec = 1000 + (strain/100.0) * ( 1000 );
    myServo.writeMicroseconds( usec );
  }
}
```

Appendix C: Project Management Plan

MQP DRA1601

Neurostimulation of C. elegans

